REVISION 2

Natural analogues of belite sulfoaluminate cement clinkers from Negev desert, Israel

ELLA V. SOKOL[1], SVETLANA N. KOKH[1], YEVGENY VAPNIK[2], VINCENT THIÉRY[3*] AND SOPHIA A. KORZHOVA[1]

[1] V.S.Sobolev Institute of Geology and Mineralogy, Siberian Branch of the RAS, prosp. Akademika Koptyuga 3, Novosibirsk, 630090, Russia

[2] Department of Geological and Environmental Sciences, Ben-Gurion University of the Negev, POB 653, Beer-Sheva 84105, Israel

[3] Mines Douai, LGCgE MPE-GCE, F-59508 Douai, France

*Corresponding author (vincent.thiery@mines-douai.fr)

ABSTRACT

Ye'elimite-larnite rocks in the Hatrurim formation of the Negev Desert, Israel, are natural analogues of belite sulfoaluminate ('BSA') cement clinkers. They have been produced by ultra-high temperature combustion metamorphism at ambient pressure of a calcareous sedimentary precursor. Their mineralogy consists of 35-50 vol% β - Ca_2SiO_4, 15-20 vol% ye'elimite, 7-15 vol% ferrites; and 15-20 vol% fluorapatite and/or fluorellestadite. A few grains of hatrurite (Ca_3SiO_5) and α' - Ca_2SiO_4 have been observed as well. The

composition of α' - and β - Ca_2SiO_4 polymorphs by EPMA are near $Ca_{1.96-1.98}Na_{0.01-0.02}Si_{0.96}P_{0.03}Al_{0.01}O_4$, whereas ye'elimite has an approximate composition by EPMA of $Ca_{3.99}Mg_{0.02}Ba_{0.01}Na_{0.02}K_{0.02}Al_{5.73}Fe^{3+}_{0.16}Si_{0.10}S_{0.97}P_{0.02}O_{16}$. The Al - content of brownmillerite $Ca_2(Fe_{1-x}Al_x)_2O_5$ ranges from x = 0.20-0.27. Fe-analogue of shulamitite ($Ca_3Fe_2TiO_8$) contains up to 15.1 wt% TiO_2. Ye'elimite-larnite rocks were derived from chalky sediments by burning of combustible gas with a T_{max} at 1 200-1 350 °C. The mineral content, microstructure and texture/fabric of the ye'elimite-larnite rocks imply that chalky and/or marly sediments with randomly distributed clay, phosphorite, and gypsum may be utilised as cheap naturally homogenised and pulverised mixtures for industrial production of BSA cement clinker, as an environment-friendly alternative to ordinary Portland cement ('OPC').

Key-words: ye'elimite-larnite rocks, sulfoaluminate clinkers, Ca_2SiO_4 polymorphs, marly raw materials, combustion metamorphism.

INTRODUCTION

Belite sulfoaluminate ('BSA') cements are generally friendlier to the environment compared to ordinary Portland cements ('OPC') for a number of reasons, notably: (1) lower CO_2 emission by about 10-25 wt% assuming alite is nearly completely exchanged for Ca_2SiO_4 polymorphs (Senff et al. 2011, Justnes 2012); (2) lower clinkering temperatures (1 200-1 350 ºC compared to 1 400-1 450 ºC in OPC) and thus reduced fuel demand for burning (Taylor 1997); (3) lower alkali-content of the produced clinker beneficial for prevention of deleterious alkali-aggregate reaction in concrete (Broekmans 2012); (4) application of industrial wastes and/or by products as valuable mineral resources, eg. fluidised-bed combustion wastes, low-quality pulverised coal fly ashes,

gypsum from flue-gas desulfurisation (Zhang et al. 1999, 2012, Quillin 2001, Gartner 2004, Gartner and Li 2006, Cuberos et al. 2010, Idrissi et al. 2010, 2011, Justnes 2012, Aranda et al. 2013). These environmental aspects also bring additional commercial advantages, as (re-)use of wastes, by-products and/or less pure natural raw materials is generally cost-saving.

Raw meal formulations for BSA clinkering as well as composition and performance of the product clinker constituents have been discussed extensively in the literature, eg. Gartner and Li (2006), Idrissi et al. (2010, 2011), Carmen Martín-Sedeño et al. (2010), Cuberos et al. (2010), Pöllmann (2010, 2012), among many others. The most challenging lacunas in current knowledge yet to be resolved comprise:

1. inexpensive formulations for raw meal to obtain optimal proportions of ye'elimite ($Ca_4Al_6O_{12}[SO_4]$, or $C_4A_3S\square$ in CAS cement notation (see Bogue and Steinour, 1961, and Table 1), essential for early strength development in BSA concrete, and α′ - Ca_2SiO_4 and/or β - Ca_2SiO_4 polymorphs (C_2S in CAS notation) delivering good long term strength.
2. minimize or inhibit formation of non-hydraulic phases like eg. gehlenite (C_2AS), sulfospurrite ($C_5S_2S\square$), spineloids (MA), magnesioferrite (MF), and various F and/or P - bearing compounds notably fluorapatite, fluorellestadite, and cuspidine etc.
3. the effect of main and trace elements in the raw meal on the phase composition of the product clinker and stabilisation/destabilisation of individual mineral constituents.
4. the partitioning of trace elements inherited from raw materials in and among clinker constituents.

The combined effect of multiple chemical elements on crystalline clinker phase stability, melting point position, and hydration behavior is very complicated and analytically challenging to unravel. Thus, clinker minerals are typically investigated in experiments with a limited number of well-characterized phases, for various compositions (Fukuda and Taguchi 1999, Benarchid et al. 2004, 2005, Marinho and Glasser 1984, Fukuda and Ando 2002).

Ye'elimite-larnite (YL) rocks studied here occur in the Negev Desert (Dead Sea region), where anhydrous clinker phases have survived due to the extremely arid climate (Goldreich 2003). They are of natural origin and were formed by decarbonation and sintering of marine calcareous carbonate sediments with complex initial mineral content and chemical composition. The chalky and/or marly precursor rocks contain variable amounts of gypsum, phosphorite, and clays, with variable abundances of minor and trace elements like eg. P, S, Se, F, Br, Sr, Ba, V, Cd, Cr, Ni, Cu, Ag, Zn, U, and others (Bogoch et al. 1999, Techer et al. 2006, Fourcade et al. 2009, Sokol et al. 2010, 2012, Fleurance et al. 2013). Its metamorphic rock product can be regarded as the equivalent of a natural experiment of BSA clinker production. The relatively coarse grain size allows detailed petrographic assessment of crystal habits and spatial distribution at microscale, as well as mineral chemistry and element partitioning between phases. The thermal regimes of industrial clinker production are compared with combustion metamorphism of sediments upon natural burning of fossil fuel under geological conditions, by applying Ono's method (Ono 1980a, 1980b) to the ye'elimite-larnite rocks. Improved knowledge of the mineralogy of these natural ye'elimite-larnite rocks may contribute to the utilization of marl/impure carbonate rocks as raw materials for industrial clinker production.

GEOLOGICAL AND PETROLOGICAL BACKGROUND

Industrial cement clinkers are similar to natural carbonate and/or marl sedimentary rocks subject to changes under high and ultrahigh temperatures at low pressure. These rocks consist of silicates with high Ca:Si ratios, fully dehydrated and decarbonated, which belong to the ultrahigh temperature low-pressure spurrite-merwinite-larnite metamorphic subfacies (Grapes 2011). Unlike industrial technologies, the conditions of high- to ultrahigh-temperature (up to 1 000-1 500 ˚C) and low (about ambient) pressure very rarely occur in nature. At present only two natural heat sources are known to cause metamorphism of sediments under such conditions. One is basaltic magma that entrains sedimentary rock fragments on its way to the surface (Reverdatto 1973, Grapes 2011, Sharygin 2012). The other source is heat released during the large-scale burning of fossil fuel (coal, oil shale, gas, and oil). Burnt and fused sediments produced by these natural fires are called combustion metamorphic (CM) or pyrometamorphic rocks (Church et al., 1979, Gross 1977, Bentor et al. 1981, Cosca and Peacor 1987, Cosca et al. 1989, Sokol et al. 2005, Grapes 2011, Grapes et al. 2009, 2011, 2013).

The so-called Hatrurim Formation (also known as the Mottled Zone) complexes in the vicinity of the Dead Sea are an exceptional occurrence where the similarity of combustion metamorphism to technological clinkering, in both processes and products, is more obvious than anywhere else. The areas contain abundant and diverse calcium-rich CM rocks with typical clinker mineralogy found in whole outcrops. Gross (1977, 1984) and Kolodny (1979) were the first to recognize the similarity of these rocks with cement clinker. Some minerals (spurrite, larnite, rankinite, wollastonite, parawollastonite, gehlenite, mayenite, brownmillerite, various Ca ferrites, and fluorellestadite) are widespread and rock-forming minerals in the Hatrurim CM rocks. Other typical clinker phases such as nagelschmidtite, ye'elimite, pseudowollastonite (α - CS in CAS notation), periclase (M), merwinite (C_3MS_2), hatrurite (alite, C_3S), α' - Ca_2SiO_4 (analogue of type I

belite), bredigite (C_7MS_4), and grossite (CA_2) are rare (Table 1) (Fleischer et al. 1978, Gross 1977, 1984, Sokol et al. 2008, 2010, Kokh 2010, Seryotkin et al. 2012).

Bentor et al. (1963), Kolodny (1979), Burg et al. (1991, 1999), Khoury and Nassir (1982), Khoury and Milodowski (1992), Khoury (2007) and Techer et al. (2006), interpreted the Hatrurim Formation complexes as products of *in situ* combustion of low-calorific fuel, specifically, disseminated bituminous matter in marine chalk. Gilat (1998), Vapnik et al. (2007), Sharygin et al. (2008, 2013), Seryotkin et al. (2012), Sokol et al. (2008, 2010, 2011), attribute CM events within the Hatrurim Formation complexes to local breakthrough and ignition of high-calorific hydrocarbon gases, mainly methane. It is the calorific capacity of the fuel responsible for combustion metamorphism of sediments that is relevant to the current study. Although the origin of the Mottled Zone complexes has been a subject of much discussion, the larnite-bearing CM rocks are generally agreed to result from high-temperature (900 – 1 200 ºC) solid-state reactions of decarbonation and sintering (Kolodny and Gross 1974, Gross 1977, 1984, Matthews and Gross 1980, Burg et al. 1991, 1999, Sharygin et al. 2008, 2013, Sokol et al. 2010, 2011). According to isotopic and geological evidence, most CM rocks in the Hatrurim basin formed within the time spans of 2.5 – 3.8, 1.6 – 5.4, and 1.2 – 1.7 Ma (Gur et al. 1995).

The Hatrurim Basin complex (11.3 × 7.3 km; 47.8 km^2) is located in the northern Negev Desert (31º12´ N, 35º16´ E) in the south-western side of the Dead Sea within Zohar-Mesada tectonic block (Fig. 1). The Hatrurim Formation rocks were observed at several levels of the section (mainly in the northern and central part of the area at depths from 30-40 to 120 m) (Burg et al. 1991, Hirsch et al. 2008). Larnite-bearing rocks occur at several levels, mainly in the northern and central parts of the area. In the lower part of the section within 20 m above the base, larnite-bearing rocks are from a few tens of cm to 1-2 meters thick and closely associated with gehlenite hornfels. Both the larnite and gehlenite rocks

may grade into so-called pseudo-conglomerates by subsequent hydration (Gross 1977, 1984, Sharygin et al. 2008, 2013). The pseudo-conglomerates consist of "pebbles" and "cobbles" (1 - 2 to 15 – 20 cm in diameter) of CM relics in a light-coloured matrix of hydration and/or carbonation products (mainly calcite, aragonite, gypsum, and ettringite, with lesser amounts of tobermorite, jennite, afwillite, and hydrogarnet; Table 2). The matrix also contains relic opaque minerals or occasionally grains of gehlenite and rankinite. The secondary phases form distinct laminated aggregates that coat the pseudo-conglomerate "pebbles" to form layered shells (Fig. 2). In the upper part of the section, larnitic rocks occur as isolated mottles (to 10 m across) among strongly altered rocks. On hilltops, monolithic larnite rocks make up separate isometric massive blocks, slabs or form cliff scarps, up to 50 m across and 5 m thick.

SPECIMEN PREPARATION AND ANALYSIS

The ye'elimite-larnite rocks were studied by optical thin section petrography, with scanning electron-microscope (SEM) for additional detail, and/or X-ray powder diffraction (XRPD) for quantification of main constituents. In-situ mineral chemistry was assessed by electron-microprobe (EMPA) at the V.S. Sobolev Institute of Geology and Mineralogy – IGM in Novosibirsk. Bulk whole-rock compositions of main elements were analyzed by inductively-coupled plasma atomic emission-spectrometry (ICP-AES) at IGM, of trace elements by synchrotron-radiation X-ray fluorescence (SR-XRF) at the Institute of Nuclear Physics in Novosibirsk.

Thin sections of YL rocks were prepared using standard equipment and protocol (eg. Humphries 1992). Polished thin (200–300 μm) sections in epoxy resin were used for optical studies. The thin-section top surface was polished and the sections were studied with both transmitted and reflected light. Petroleum was used for coolant/lubricant to

accommodate preparation of hydrophobic materials. Thin sections were finished by polishing using 0.25 μm diamond paste. Prior to assessment in SEM, polished sections were sputter coated with ~30 nm gold – Au, for chemical analysis using EMPA as well as for elemental mapping using SEM with carbon – C.

For mineral identification by XRD all natural sample materials were crushed and pulverized under iso-propanol. After overnight drying at 50 °C in a covered petri dish and homogenization, powders were front-loaded in a dimpled sample holder and the surface finished with a glass slide. Mounted specimen of all the rocks mentioned in the Table 2 were analyzed in a Bourevestnik DRON-3 diffractometer with Bragg-Brentano geometry, using bulk CuKα radiation with $\lambda = 1.54178$ Å. Scans were recorded from 6-60 °2θ at 0.05 °2θ increments with 5 s scanning time per step. Mineral phases were identified with Bourevestnik proprietary software using ICDD card file data. From these diffractograms it is possible to identify the presence and relative amounts of the main crystalline phases: larnite (C_2S), ye'elimite ($C_4A_3S\square$), gehlenite (C_2AS), fluorapatite ($C_{10}P_4\,\overline{F}$) or fluorellestadite ($C_{10}S_3\overline{S}_3\,\overline{F}_2$) and brownmillerite ($C_4AF$), as well as identify minor amounts of secondary tobermorite and gibbsite. The obtained phase compositions are close to those identified by the SEM, EMPA, and optical studies (Table 2).

After then three principal rock samples (YV - 410, YV - 411, and YV - 412) were characterized through X-ray powder diffraction in Mines Douai, in Douai, France. XRD was conducted in a Brüker D8 diffractometer with a Co Kα radiation (1.78 Å) source in 10–80 °2θ range at 0.05 °2θ increments with 5 s scanning time per step range. The pattern indexation has been carried out using Bruker Diffrac Eva software. Fig. 3 shows the selected (characteristic) range of the XRD plots for the comparative YL rocks.

Microfabric and phase distribution were assessed in LEO 420 SEM and JEOL JSM6380LA scanning electron-microscope instruments on both Au- and C-coated polished

thin sections, at chamber vacuum pressure 10^{-5} Torr (~0.01 Pa). Both instruments were operated at 10 kV and 2.0 nA beam current (Faraday cup). Images were acquired in both SE and BE modes.

In-situ chemical compositions of individual mineral grains were assessed using CAMECA Camebax-Micro and JEOL JXA-8100 microprobe instruments, on C-coated polished thin sections. Chamber vacuum was kept at 10^{-6} Torr (~0.001 Pa) or better. Both instruments were equipped with a single EDS spectrometer and five WDS spectrometers with LiF, PET, or TAP crystals. Mineral compositions were analyzed at 20 kV, beam current of 15-30 nA, acquisition time of 10 s, and beam diameter at the point of incidence on the specimen surface of 2-3 μm. The analyzed grains were > 10 μm in size. For the minerals sensitive to elemental species migration and evaporation upon beam exposure (particularly ye'elimite and fluorellestadite) the beam was defocused to 5-10 μm in diameter, current reduced to 10 nA, and counting time reduced to 5 s. Measurement of F was allocated to a WDS-TAP detector at the start of an analytical run, to further minimize evaporation artifacts (see Morgan and London 2005). Peak overlaps for CaK_{β}-PK_{α} and SiK_{α}-SrL_{α} were automatically compensated by the instrument software, and matrix correction using ZAF algorithm was applied to raw data prior to recalculation into major oxides. Analytical accuracy is within 2 %-relative for >5 wt% elements, and about 5 %-relative for < 2 wt% elements, notably Na, K, Cl, and F. Data and net detection limits are tabulated in wt%. Oxide contents are recalculated into **a**toms **p**er **f**ormula **u**nit – **apfu** following routine procedures outlined in eg. Deer et al. (1992) and Papike (1987, 1988).

Samples for bulk whole-rock geochemical analysis were crushed in a jaw breaker to <0.5 mm and homogenized. Next, ~10 g aliquots were pulverized in a vibratory disc mill with agate lining, and homogenized. The aliquots were well representative because all rocks were fine-grained, with uniformly distributed main and accessory phases (see the

section *Sample Materials* below and Fig. 5). Exactly 0.2 g of sample powder was mixed with 0.6 g of lithium metaborate in a platinum crucible. Samples were fused in a muffle furnace at 1050 ^{o}C for 20 min. Each sample was removed from the furnace, placed directly into 100 ml of 3.5 wt% HNO_3, and was mixed on a magnetic stirrer until complete dissolution (usually 20-30 min). The solutions were then transferred into 250 ml volumetric flasks and made to volume with deionized distilled water. Each sample was further diluted prior to analysis by adding 3.5 wt% HNO_3. The final solution was fed into IRIS Advantage (ThermoJarrell International Corporation, USA) instrument at IGM (Novosibirsk) for analysis by ICP-AES. For details of the analytical procedure see (Shatsky et al. 2006). The trace elements were analysed at the Siberian Synchrotron and Terahertz Radiation Center (SSTRC) based on the laboratories of Budker Institute of Nuclear Physics, Novosibirsk, using precise synchrotron radiation X-ray fluorescence analyses (SR XRF) with EDS (energy-dispersion spectroscopy), at 23 kV and 42 kV excitation energy (Phedorin et al., 2000). The instrument accuracy of the SSTRC analyser was previously estimated (Zvereva, 2009) to range from 5 % to 20 %, increasing towards lower concentrations to the maximum at ≤10 ppm. The element abundances were measured in 50 mg fine powder (< 20 μm) in samples compressed into 6 mm pellets at 120 – 150 kg/cm^2. All measurements were run in triplicate (in three different pellets) and quoted as the averages. The difference between element abundances within the triplets did not exceed the relative error of each determination. Data and net detection limits for major oxides and trace elements are tabulated in wt% and ppm [mg/kg], respectively (Tables 3 and 4).

SAMPLE MATERIALS

Fresh ye'elimite-larnite rocks were sampled from a huge stack of prehistoric knapped waste and bifacial tools which was discovered by Dr. Ye. Vapnik in 2009 (Vapnik and Vardi 2013, Vardi and Cohen-Sasson 2012, Zenin 2012). The stone tools, fabricated mostly from YL rocks or less often from gehlenite-larnite hornfels, were found on the top of Mount Har-Parsa (31°12'38,71" N; 35°16'57,81 "; h = 299.7 m) in the central Hatrurim Basin. The tool-makers apparently preferred Ca - rich CM rocks to abundant cherts available in the vicinity. Massive larnite and gehlenite varieties crop out in small but numerous cliffs upon and near the flat top of Har-Parsa, while ye'elimite-larnite rocks occur more often as "balls" coated with secondary hydration and carbonation products (Figs. 2 and 4).

The Har-Parsa fresh ye'elimite-larnite rocks are deep brown, grey to black, fine-grained, dense, and homogeneous. The YL rocks studied here are compositionally uniform with least variation in contents (in diminishing order; see Table 3) of CaO, SiO_2, Al_2O_3, Fe_2O_3, P_2O_5, MgO, and TiO_2, and significant variation in SO_3 (~ 4 ×) Na_2O (~ 5 ×), and K_2O (> 20 ×). Their contents (in diminishing order; see Table 4) in Sr, Ba, Zn, Cr, Ni, V, Se, and U are generally interpreted as inherited from the sedimentary protolith. The Har-Parsa YL rocks consist of 35-50 vol% larnite, 7-15 vol% of opaque minerals (brownmillerite, Fe^{3+} - analogue of shulamitite (C_3FT in cement notation), magnesioferrite); 15-20 vol% fluorellestadite or sulfate-bearing fluorapatite, and 15-20 vol% ye'elimite (Figs. 5 and 6).

S*ample YV-410* is a stone tool manufactured from a homogeneous, massive, microcrystalline (5-30 μm) dark grey and greenish hornfels. The main phases are gehlenite, larnite, ye'elimite, and fluorapatite. The minerals are uniformly distributed, except opaque phases (up to 200 μm). Ye'elimite contains larnite, hatrurite, and opaque minerals as oval inclusions. The sample also contains a few small grains of hatrurite. Some of the ye'elimite

grains has decomposed and gave way to $Al(OH)_3$ formed in their place. Tobermorite is present in trace amounts and is identified from the strongest X-ray diffraction line (2Θ 10.8° (Cuk_α)). Opaque minerals are fresh and show no indications of hydration/oxidation.

Sample YV - 411 is a stone tool and *YV - 412* is the same rock collected from the outcrop. The rocks are homogeneous, massive, microcrystalline (5-30 μm) with a deep brown colour and typical hornfels texture. Mineral distributions is relatively uniform (Fig. 5), with larnite, ye'elimite, fluorapatite (YV - 411), and fluorellestadite (YV - 412) being the rock-forming phases. All minerals (except opaques) host numerous mineral inclusions and, in turn, may be hosted by any of the other minerals. The rock contains larnite (β - Ca_2SiO_4) as rock-forming mineral and α′ - Ca_2SiO_4 as sporadic grains. Among the opaque phases, brownmillerite with low Ti is predominant, magnesioferrite is secondary; Cr - bearing barite is an accessory. Accessories in YV - 412 include periclase, two rare selenides, namely Cu_2Se (berzelianite or bellidoite), eucairite (CuAgSe), and vorlanite ($(CaU^{6+})O_4$) or "protovorlanite" $CaUO_4$, recently discovered uranium minerals (Galuskin et al. 2011, 2012, 2013, Othmane et al. 2013). Slight hydration is evident in some ye'elimite grains that are replaced by gibbsite (Fig. 6). Trace amounts of tobermorite is the hydration product of dicalcium silicates.

Sample *YV - 413* is a man-made breccia of YL rock artefacts of an unusual origin. Gallets of larnite-bearing (mainly YL) rocks that have remained stacked at the tool production site have become cemented with secondary calcite to form monolithic breccias due to hydration and carbonation during weathering. As a result, each gallet has acquired a thin coating of fine secondary calcite. Immediately beneath the calcite coating, there is a thin (0.1-0.2 mm) zone of hydration where larnite has been completely consumed. The interior of gallets larger than 5 mm are not visibly weathered (Fig. 5).

MINERAL CONTENT AND CHEMICAL COMPOSITION

Dicalcium silicates. Both α´ - Ca_2SiO_4 and β - Ca_2SiO_4 (C_2S; for CAS notations see table 1) polymorphs occur in the YL rocks. Larnite (β-Ca_2SiO_4) is a main phase (up to 40-50 vol%) and is similar in appearance to type II belite from production clinkers (Figs. 6-8) (Taylor 1997, Campbell 1999). It forms rounded grains, typically 20 to 40 μm (rarely up to 50 μm) and shows a single set of distinct striations, which are polysynthetic twins after (100) or (010) arising from α'_L - Ca_2SiO_4 to β - Ca_2SiO_4 transformation (Taylor 1997). In thin section larnite appears colourless or greyish. Larnite grains are free from zonation, cracks, pores, or overgrowth structures; in some cases they contain ye'elimite inclusions and overgrowth brownmillerite and/or an Fe^{3+} - analogue of shulamitite. Silica in the larnite (32.1-34.5 wt%) is below the theoretical value (34.9 wt%), and is typically substituted by P (0.45-1.92 wt% P_2O_5) or less often by Al (0.08-0.29 wt% Al_2O_3). Sulphur occurs in a few grains (to 0.14 wt% SO_3) (Table 5). The lack of significant correlation between Al and S argues against the $2Al^{3+} + S^{6+} \rightarrow 3Si^{4+}$ substitution inferred for clinker belite (Taylor 1997). CaO is also below the theoretically predicted amount (63.4-64.7 wt%) in ideal larnite, because of substitution of Na, K, Sr, Ba and Mg. Sodium correlates with the whole-rock soda content and reaches 0.62 wt% Na_2O, with the rock containing 0.18-0.47 wt% Na_2O. Potassium is up to 0.18 wt% K_2O. Sr, one of the most important industrially-used stabilisers of α-, α'-, and β - Ca_2SiO_4 polymorphs, does not exceed 0.25 wt% SrO, and its average bulk rock contents are 1 400-2 000 ppm. Barium, another stabiliser of β - Ca_2SiO_4, was found in a few grains (up to 0.26 wt% BaO), as well as magnesium and iron (up to 0.31 wt% MgO and 0.41 wt% FeO). V_2O_5 approaches its detection limit (up to 0.08 wt%). Thus, total impurities in larnite from YL rocks are 2-3 wt%, which distinguishes them from high-temperature clinker belite (mainly α- and α'-

Ca_2SiO_4) with typically 4-6 wt% of substitute oxides, usually P_2O_5, Al_2O_3, Fe_2O_3 or Na_2O (Taylor 1997, Campbell 1999, Fukuda and Taguchi 1999, Benarchid et al. 2004, 2005).

The phase **α´-Ca_2SiO_4**, not yet confirmed as a new natural mineral species and sometimes misnamed bredigite ($Ca_7Mg[SiO_4]_4$ – C_7MS_4, see Taylor, 1997 for details), is extremely rare in the studied YL samples. It was identified on the basis of its rounded morphology in a single YL sample, YV - 413. The round grains have indistinct crystal faces and show two sets of intersecting lamellae, indicating an affinity to a natural equivalent of type I belite. Two types of symmetry-related domain structures of β-form are set in a α' - Ca_2SiO_4 matrix. The striations intersect at an angle of 60 ° or 120 ° in cross-sections perpendicular to the $c_{\alpha'}$ - axis of the host. In other sections, lamellae cross at 23 °, 15 ° and 27 °. The orientation relationship between the host α' - Ca_2SiO_4 and the β - form lamellae is $\{11\bar{2}0\}_{\alpha'} \parallel \{100\}_{\beta}$ and $<0001>_{\alpha'} \parallel <010>_{\beta}$. Most β - lamellae show {100} twining (Fig. 7). The orientation of β - form lamellae in host α' - Ca_2SiO_4 are identical to microtextures fixed in cement belites (Ca_2SiO_4 solid solutions) by Fukuda and Maki (1989, 1993) and Fukuda (2001) (Fig. 8). The two sets of lamellae intersect at 60° and have been generally attributed to the α - Ca_2SiO_4 to α´ - Ca_2SiO_4 inversion that survive only on quenching at temperatures above 1 280°C (Fukuda 2001). The average composition of the α´ - Ca_2SiO_4 polymorph determined by EMPA (using a beam diameter of 2 μm which covers an area of < 4 μm) is (in wt%) 63.6-64.1 CaO, 34.2-35.1 SiO_2, 0.38-0.41 Na_2O, 0.09-0.14 K_2O, 0.60-0.99 P_2O_5; Mg. Cr, and V are about at their detection limits; S and Sr are undetected.

Hatrurite (Ca_3SiO_5 – C_3S) was identified only (by EDS in sample YV - 410), with the composition (wt%) 51.8 Ca, 11.1 Si, 1.1 Al, 0.40 Mg, 0.60 P, and 35.0 O (Σ = 100.0), coincides well with calculated values for pure the Ca_3SiO_5 of 52.66 wt% Ca, 12.30 wt% Si,

and 35.04 wt% O (Σ = 100.0). The mineral occurs sporadically as etched grains < 10 μm, too small for analysis with additional methods.

Calcium sulfoaluminate ($Ca_4Al_6O_{12}SO_4$ – $C_4A_3S\square$) known as the mineral **ye'elimite**, is extremely rare in nature. Until recently, it was found nowhere else but in the Hatrurim CM rocks where it was originally discovered (Gross 1983, Sharygin et al. 2008, Sokol et al. 2010, Kokh 2010, Galuskin et al. 2013); subsequently it was found in metacarbonate xenoliths from the Ettringer Bellerberg volcano in the East Eifel, Germany (Sharygin 2012). In the analyzed YL samples, ye'elimite is a rock-forming mineral (up to 15-20 vol%) forming colourless rounded grains of 5-50 μm diameter (Figs. 5 and 6). Grains with up to 2.90 wt% Fe_2O_3 in sample YV - 411 have an ochre tint extending from rim to core. Ye'elimite always contains numerous inclusions of Ca_2SiO_4 and sporadic opaque minerals. The mineral commonly remains fresh but sometimes contains microscopic vugs filled with aluminium hydroxide.

The ye'elimite composition (wt%) differs slightly from its ideal formula $Ca_4Al_6O_{12}(SO_4)$, with 45.6-48.0 Al_2O_3, 35.2-36.9 CaO, and 11.2-12.7 SO_3 (Table 6); SiO_2 (0.42-1.80), Fe_2O_3 (1.80-2.90), and SrO (0.20-0.47) are impurities. Occasionally, ye'elimite may contain (wt%): BaO (up to 0.94), K_2O (to 0.43), P_2O_5 (to 0.26), Na_2O (to 0.23), and Cr_2O_3 (to 0.17); Ti, Mg, and V in all samples, as well as K, Na. Cr, and P in some samples, are below or about detection limit. No fluorine or chlorine have been found. By analogy with $Ca_4Al_{(6-2x)}Fe_{2x}SO_{16}$ with $x = 0$, 0.2, and 0.5 synthesised by (Idrissi et al. 2010, 2011), the natural mineral may be considered as calcium sulfoaluminate doped with Fe^{3+} at $x_{max} \sim 0.1$.

Fluorapatite $C_{10}P_4$ $\overline{F}$ and fluorellestadite $C_{10}S_3$ $\overline{S}$ occur as the largest crystals (from 50 up to 200-400 μm) in the YL rocks and are crowded with inclusions of larnite, ye'elimite, and opaque minerals (Figs. 5 and 6). Small crystals are anhedral. Prismatic

habits were only noted in a few of the largest crystals. Both minerals are solid solutions with nearly constant (wt%) CaO of 55.0–56.7 and variable P_2O_5 (10.7–28.3), SO_3 (7.82–16.6), SiO_2 (5.48–14.2), and F (2.52–3.45). The main impurities (wt%) are SrO (0.17-0.34), V_2O_5 (0.12-0.58), and FeO (0.04-0.33); Cl was below detection limit (< 0.03). Minor amounts of Al_2O_3 (up to 0.11 wt%), and Na_2O (up to 0.09 wt%) were present in some grains. Fluorapatite generally contains only slightly more total impurities than fluorellestadite (~ 1 wt% against ~ 0.7 wt%) (Table 7). Unlike zoned fluorellestadite from CM rocks of coal fire sites (Zateeva et al. 2007), those from YL rocks are homogeneous.

The **opaque minerals** in YL rocks are mainly brownmillerite ($Ca_2(Fe_{1-x}Al_x)2O5$ – $C_2A_xF_{1-x}$) and an Fe^{3+} - analogue of shulamitite ($Ca_3Fe_2TiO_8$ – C_3FT). Both minerals are light- to dark- and red-brown in transmitted light. Brownmillerite is relatively abundant (up to 10 vol%) and forms irregular or prismatic grains and intergrowths (up to 300 μm). The Fe^{3+} - analogue of shulamitite is rare (1-5 vol%) and form long-prismatic crystals as well as anhedral grains (up to 20 x 5 μm) (Figs. 5 and 6). The mineral was discovered in CM ye'elimite-larnite rocks (Sharygin et al. 2008, 2013) and in xenoliths in ignimbrite from the Northern Caucasus, Russia (Galuskin et al. 2011). The compositions (wt %) of the Fe^{3+} - analogue of shulamitite are CaO (42.2-42.8), TiO_2 (16.1-17.9), Fe_2O_3 (30.9-35.1), and Al_2O_3 (4.65-5.22), while other major oxides are present as impurities: 0.70-2.67 SiO_2, up to 0.54 MnO, to 0.45 MgO, and to 0.2 Cr_2O_3. Grains of the Fe^{3+} - analogue of shulamitite appear homogeneous in BSE images and are free from reaction or overgrowth rims. It survives intact akin to water non-reactive perovskite-like phases $CaFe_{1-x}Ti_xO_{3-d}$ and particularly C_3FT in cement clinkers (Stöber et al. 2013).

The composition of brownmillerite $Ca_2(Fe_{2-x}Al_x)O_5$ varies in a range of $x = 0.40$–0.54. Impurities (wt%) are SiO_2 (0.71-1.93), TiO_2 (2.12-2.99). Cr_2O_3 (0.19-0.66), and MgO (0.63-0.86). Concentrations of other oxides are usually less than 0.07 wt% (Table 8). Thus,

brownmillerite from different YL samples is compositionally similar to those from combustion metamorphic and pyrometamorphic metacarbonate rocks from elsewhere (Sharygin et al. 2008). They are also close to Al-rich compositions of $Ca_2(Fe_{2-x}Al_x)O_5$ solid solution ($0.46 \leq x < 0.56$) belong to a space group *Pnma* (Redhammer et al. 2004, Stöber et al. 2013). Whereas solid solutions with higher Al^{3+} concentrations $0.57 \leq x$ belong to body-centered space group *I2mb* (Redhammer et al. 2004, Stöber et al. 2013) have not been found (detected) in YL rocks.

A typical brownmillerite in ordinary Portland cement clinkers differs markedly from that of C_4AF (in wt%: 46.1 CaO; 21.0 Al_2O_3; 32.9 Fe_2O_3), contains about 10 wt% of impurities and has much lower Fe_2O_3. Its average composition is $Ca_2AlFe_{0.6}Mg_{0.2}Si_{0.15}Ti_{0.05}O_5$, being derived from that of C_4AF by substituting Mg^{2+} and equal amounts of Si^{4+} and Ti^{4+} for Fe^{3+} (Taylor, 1997). In calcium aluminate cements enriched in TiO_2 ferrite phases show higher Fe/Al ratios and can uptake large quantities of trivalent manganese up to ½ of Fe^{3+} ions in the octahedrally coordinated position (Stöber et al. 2013). Mn^{3+} in brownmillerite from Portland cement clinkers can completely replace Fe^{3+} or up to 60 %-relative of Al^{3+} (Taylor 1997).

An average YL brownmillerite composition is $Ca_{1.96}Mg_{0.04}Fe_{1.38}Al_{0.47}Si_{0.04}Ti_{0.08}O_5$. Like brownmillerite from cement clinkers, the natural counterparts show little or no substitution for Ca^{2+}. Si, Mg, and Ti in natural brownmillerites are impurities with Mg mainly concentrated in magnesioferrite and Ti in Fe^{3+} - analogue of shulamitite (Tables 2 and 8). The analyzed brownmillerites have almost no Mn, which is very low in the sedimentary protolith and YL rocks (0.01-0.26 wt% MnO) (Table 3).

Magnesioferrite occurs interstitially as isolated grains (up to 10 μm) and as intergrowths (up to 40 × 60 μm). Fe_2O_3 is 61.4-64.7 wt% and MgO is 19.8-21.4 wt%; impurities are CaO (0.45-1.23), TiO_2 (0.33-0.40). Cr_2O_3 (0.8-1.63), MnO (up to 0.46), NiO

(to 0.41), and ZnO (to 0.81). Sample YV - 412 also contains oval grains of *periclase* (≥ 5 μm) with the impurities of 0.95-2.62 wt% FeO, 3.13-3.60 wt% NiO, and 1.85-2.58 wt% ZnO. *Barite* is found as anhedral grains (up to 30 μm) in interstitial areas and contains (in wt%): CaO (0.57-1.05). Cr_2O_3 (0.47-1.01), and SrO (0.47-0.77).

DISCUSSION

Bulk whole-rock compositions of ye'elimite-larnite rocks and BSA clinker

Compositions of the YL rocks differ markedly from those of BSA clinker from the Chinese cement industry produced with bauxite known as the TCS series (Zhang et al. 1999, 2012), in that they have higher SiO_2. CaO, and P_2O_5 contents, and lower Al_2O_3, TiO_2, MgO, and SO_3 contents. Nevertheless, the YL rock compositions fall within the composition range of BSA cement clinker obtained by sintering homogenised mixtures of pulverised limestone, clay, and gypsum at T = 1 150-1 350ºC (Gartner and Li 2006) (Table 3). According to the patent claim, the optimum phase composition of BSA cement clinker includes 15-35 vol% brownmillerite – calcium aluminate$_{ss}$ ($C_2A_xF_{1-x}$, x = 0.2 - 0.8), 45-65 vol% belite (both α′- and β - Ca_2SiO_4), and 20-30 vol% ye'elemite, and lesser amounts of anhydrite, alkaline sulfates, perovskite, gehlenite, and periclase (0.1-10 vol% in total). The mixture also contains boron which promotes the primary formation of α′ - Ca_2SiO_4.

BSA clinkers and YL rocks are similar both in chemistry and mineralogy (Table 9). However, the Har-Parsa CM rocks contain mostly the β - Ca_2SiO_4 polymorph while their industrial counterparts may contain either β- or γ - Ca_2SiO_4 forms (Zhang et al. 2012), or α′ - Ca_2SiO_4 (Gartner and Li 2006). The micro-structure of natural larnite, with a single set of polysynthetic twins, indicates heating in the field of α′ - Ca_2SiO_4 stability followed by α'_L - Ca_2SiO_4 to β - Ca_2SiO_4 transformation during cooling (Taylor 1997, Campbell 1999,

Fukuda 2001). This inference is supported by the presence of a few α´ - Ca_2SiO_4 grains in the analyzed YL samples and the absence of γ - Ca_2SiO_4.

Generally, the homogeneous and monolithic structure of YL rocks from Har-Parsa, as well as the fact that early humans used them for making bifaces tools, which have to be extremely hard and heavy, provides evidence of combustion metamorphism under conditions especially favourable for the β - Ca_2SiO_4 stabilization. On the other hand, the Hatrurim Formation may have originally included Ca-rich CM rocks with γ - Ca_2SiO_4 as well, because slow cooling occurred at temperatures ($T \leq 500$ ºC) corresponding to the β - Ca_2SiO_4 to γ - Ca_2SiO_4 polymorphic transition (Yamnova et al. 2011). The densities of β - Ca_2SiO_4 ($P2_1/n$) and γ - Ca_2SiO_4 (*Pbnm*) polymorphs are 3.28 g/cm^3 and 2.97 g/cm^3, respectively, and the β to γ transition is known to cause considerable volume expansion, the expansion stress being sufficient to shatter or pulverise clinkers (Taylor 1997). As Zhang et al. (2012) have shown, the pulverisation ratio in a slowly cooling BSA clinker destabilised with impurities of Fe_2O_3 and Al_2O_3 in β - Ca_2SiO_4 approached 85 %-relative, when the β - Ca_2SiO_4 to γ - Ca_2SiO_4 transition ratio was about 40 %-relative; it reached 20 %-relative at as low as 4.8 %-relative γ - Ca_2SiO_4 and the ratio β - Ca_2SiO_4 /γ - Ca_2SiO_4 = 5. Therefore, such self-pulverising rocks obviously should have a very short existence in the natural environment. Caused by the β - Ca_2SiO_4 to γ - Ca_2SiO_4 transition, the rocks inevitably decrepitated to powder and were dispersed by wind in the arid desert conditions, or were carbonated and sulphatised during periods of more humid climate. Whatever the natural setting, CM rocks that were originally rich in the high-temperature Ca_2SiO_4 polymorph and then cooled down slowly at $T \leq 500$ºC had no chance to survive intact. Such a mechanism may explain some of the carbonated retrograde rocks of the Hatrurim Basin.

Another point of difference between YL rocks and BSA clinkers is the composition and percentages of sulphate-bearing phases. The amount of ye'elimite is 75-20 vol% in BSA clinker but is no more than 20 vol% in YL rocks, being limited by low Al in the marine chalky protolith. We found neither anhydrite nor alkaline sulphates in the Har-Parsa samples. On the other hand, biogenic fluorine-bearing apatite in the sedimentary protolith has given rise to complex calcium fluoride-sulphate-phosphates. The much lower Al in YL rocks than in the BSA clinker account for lower ye'elimite content (see above), as well as markedly larger amounts of the perovskite ($CaTiO_3$) endmember in the $Ca(Fe,Al)_2O_5$-$CaTiO_3$ pseudobinary series. Under these conditions, the Fe-analogue of shulamitite becomes a significant opaque phase in natural rocks. Minerals of secondary importance and accessories (gehlenite and periclase) in the YL rocks and BSA clinker are similar.

Element partitioning during formation of natural equivalent of BSA clinker

Calcium is the principal cation which forms eight mineral species in the studied rocks. Silica mostly resides in larnite and enters fluorapatite-fluorellestadite solid solutions. The same minerals incorporate some S as sulphate, most of the phosphate P present, and all F. Larnite (β - Ca_2SiO_4) is the next most important scavenger of P, and to ever lesser extent Na, K, and Sr. The characteristic wt% concentrations of β - Ca_2SiO_4 stabilising impurities are 0.3 P_2O_5, 0.3 B_2O_3, 1.0 Cr_2O_3, 1.2 Na_2O, and 1.5 K_2O (Zhang et al. 2012). Phosphorus is obviously the principal stabiliser of β - Ca_2SiO_4 in the sintering of natural sediments; in the larnites we studied, P_2O_5 is 0.88-1.56 wt%, which is 3-5 times its characteristic concentration (Table 5). Na_2O (0.33-0.51 wt%) and K_2O (0.06-0.11 wt%) are both within the lower limit of the β - Ca_2SiO_4 to γ - Ca_2SiO_4 transition. Chromium is absent from larnite in the natural BSA analogues, but rather resides in opaque minerals and barite,

existing as $(CrO_4)^{2-}$ -group in the latter to form barite-hashemite solid solution ($BaSO_4$ – $BaCrO_4$). Iron and aluminium, 0.13-0.17 wt% FeO and 0.12-0.29 wt% Al_2O_3 in natural larnite, show neither anti-stabilisation or shielding effects (Zhang et al. 2012) nor does it weaken the P-stabilisation of β - Ca_2SiO_4.

Al resides in ye'elimite (46-48 wt% Al_2O_3) and in opaque minerals (5-20 wt% Al_2O_3). Iron is mostly present in opaque phases and is also an important impurity in ye'elimite (2-3 wt% Fe_2O_3) and periclase (0.90-2.25 wt% FeO). Opaque minerals also concentrate almost all Mg, Ti, and Mn.

Finally, Ba, Sr, and V occur in fluorapatite-fluorellestadite solid solutions. Ni and Zn in periclase, and the incompatible elements Cu, Ag, Se, U in accessory minerals. They are the latest phases to form in the YL samples and most likely result from fractionation of the respective impurities from the growing rock-forming minerals. It suggests relatively stable growth conditions and long-term high-temperature sintering.

Thermal regime

Based on the mineralogical similarity of the Hatrurim YL rocks and BSA industrial clinker, we use Ono's method (Ono 1980a, 1980b, Maki 1994, Campbell 1999) to reconstruct the thermal regime of the natural CM samples and, more specifically, to determine relative changes in sintering conditions (T_{max}, burning time, and rates of heating and cooling) (Table 10). Clinker phases from the natural YL rocks show a number of features, namely: (i) crystal morphology with rounded larnites and prismatic ferrites; (ii) uniform distribution of minerals, including interstitial opaque phases; (iii) prevalence of the β - Ca_2SiO_4 form, with few grains of the α′ - Ca_2SiO_4 form; (iv) chemical homogeneity of larnite, ye'elimite, fluorellestadite, fluorapatite, and opaque minerals; (v) uniform distribution of impurities and absence of zonation within them. These features provide

evidence of prolonged heating of sediments at high temperature, below the C_4AF melting point (T < 1300 °C) (De la Torre et al. 2011). Inasmuch as all CM rocks studied contain ye'elimite, the temperature 1 350-1 400 °C above which it decomposes (Idrissi et al. 2010, De la Torre et al. 2011, Zhang et al. 2012) is probably the upper limit of combustion metamorphism of YL chalky protolith.

Ono's method estimates burning time for thermal processes in industrial cement clinkers of about four hours. Extrapolating this method to the natural setting, it is predicted that the YL sediment protoliths were subjected to high temperature heating for longer than four hours and probably for more than a few days. This is consistent with the duration of natural methane combustion at various CM sites (Grapes et al. 2013). Lack of high temperature recrystallisation of minerals, and their sizes being similar to phases in ordinary cement clinkers, although much smaller than in contact metamorphic spurrite-mervinite-larnite subfacies rocks (Grapes 2011), implies a single, short fuel combustion event at the Hatrurim Basin.

Preservation of a few grains of α′ - Ca_2SiO_4 in theYL rocks suggests quenching at T > 1280 °C (Maki 1994, Fukuda 2001) (Table 10). Colourless, rounded larnites with polysynthetic (100) or (010) twins and without exsolved dot-like inclusions, may survive at quenching temperatures no lower than 1 200°C. Other features, such as a high percentage of the $CaTiO_3$ component in Ca ferrites; relatively abundance of the Fe^{3+}-analogue of shulamitite; large isolated aluminate and ferrite crystals; presence of pyrrhotite, as well as Cu and Cu-Ag selenides, attest to burning and rapid quenching at T ≥ 1250 °C under moderately reducing conditions. The absence of encrustations indicates a dry environment of sintering.

In conclusion, we note that, in terms of technology, the YL rocks are a high-quality uniformly sintered clinker (Taylor, 1997, Campbell, 1999) (Table 10), with random and

uniform spatial and size distribution of its rock-forming minerals. Therefore, the YL rock protolith of fine-grained non-compacted chalky and/or marly sediments with randomly distributed clay and gypsum may be utilised as naturally homogenous starting material for the industrial production of BSA cement clinkers. Compositions can be adjusted by doping with clay, gypsum, etc., for producing BSA cements of a designed quality. The material is free from coarse quartz or feldspars which would otherwise produce belite concentration nests and heterogeneity in the clinker. Bulk composition can be adjusted as necessary by addition of clay, gypsum, etc. to meet quality requirements for BSA cements. On the other hand, local enrichment of sedimentary precursor in biogenic apatite would result in the formation of a considerable amount of fluorellestadite-fluorapatite solid solution phases (up to 15-20 vol%) in the clinker which would reduce its hydraulic capacity.

IMPLICATIONS

Ye'elimite-larnite rocks from the Hatrurim Basin, Israel, were produced by ultrahigh-temperature combustion metamorphism of calcareous marine sediments. Exposed to near surface chalky sediments were subjected to temperatures of BSA clinkering temperatures (1 200–1 350°C), under burning conditions of fuel (methane) excess relative to an oxidiser, which maintained a moderately reducing environment during annealing. Fine chalky sediments were heated uniformly and devolatilised quite rapidly (until complete exhaustion of the fluid component), which inhibited the development of a coarse grain size of the clinker minerals that formed the resultant ye'elimite-larnite rocks. The structure of the natural clinker and its mineral composition formed rapidly at peak temperatures during a single combustion event that lasted up to a few days at $1200\ °C < T_{max} \leq 1350\ °C$, followed by rapid quenching. The well-preserved clinker mineralogy of the YL rocks was due to rapid high-temperature quenching and the

extremely dry climate of the Negev Desert which prevented the unstable high temperature anhydrous mineral assemblages being extensively modified by hydration reactions. Hydration mainly affected rocks adjacent fissures to produce secondary assemblages of calcite-gypsum-ettringite, which caused expansion and disintegration of the clinkers. The unweathered hard YL rocks were especially suitable for the manufacture of large artifacts by prehistoric mankind, arguably the first representatives of *Homo* who utilise BSA clinker for practical applications.

ACKNOWLEDGEMENTS

We dedicate this paper to the hallowed memory of Dr. Shulamit Gross (1923-2012) whose inspiring talent and diligence have brought to light the mineral treasures of Hatrurim. We wish to acknowledge Associate Editor Maarten Broekmans who made a significant intellectual contribution to the present work. The authors are grateful to Dr. Stefan Stöber (Halle (Saale), Germany) and the anonymous reviewer for critically reviewing and correcting the manuscript. We further wish to thank Dr. V. Sharygin and T. Perepelova (IGM, Novosibirsk) for cooperation and helpful advice. Thanks are extended to Drs. N. Karmanov, Yu. Kolmogorov, E. Nigmatulina, and M. Khlestov for their assistance in the analytical work (IGM SB RAS, Novosibirsk). Trace element abundances were analyzed by Yu. Kolmogorov at the shared-research Siberian Synchrotron and Terahertz Radiation Centre, Budker Institute of Nuclear Physics (Novosibirsk, Russia). The study was supported by grant 12-05-00057 from the Russian Foundation for Basic Research. Research at the Har-Parsa stone workshop by Dr. Ye. Vapnik was supported by Irene Levi-Sala CARE Archaeological Foundation.

REFERENCES

Aranda, M. A. G. and De la Torre, A. G. (2013) Sulfoaluminate cement, Ed. Pacheco-Torgal, F., Jalali, S., Labrincha, J., John, V. M. (Eds.), Eco-efficient concrete (Cambridge), 488-522.

Benarchid, My. Y. and Rogez, J. (2005) The effect of Cr_2O_3 and P_2O_5 additions on the phase transformations during the formation of calcium sulfoaluminate C_4A_3S□. Cement and Concrete Research, 35, 2074-2080.

Benarchid, My. Y., Diouri, A., Boukhari, A., Aride, J., and Elkhadiri, I. (2005) Hydration of iron-phosphorus doped dicalcium silicate phase. Materials Chemistry and Physics, 94, 190-194.

Benarchid, My. Y., Diouri, A., Boukhari, A., Aride, J., Rogez, J., and Castanet, R. (2004) Elaboration and thermal study of iron-phosphorus-substituted dicalcium silicate phase. Cement and Concrete Research, 34, 1873-1879.

Bentor, Y.K., Gross, S., and Heller, L. (1963) High-temperature minerals in non-metamorphosed sediments in Israel. Nature, 199, 478–479.

Bentor, Y.K., Kastner, M., Perlman, I., and Yellin, Y. (1981) Combustion metamorphism of bituminous sediments and the formation of melts of granitic and sedimentary composition. Geochimica and Cosmochimica Acta, 45, 2229-2255.

Bogoch, R., Gilat, A., Yoffe, O., and Ehrlich, S. (1999) Rare earth trace element distributions in the Mottled Zone complex, Israel. Israel Journal of Earth Sciences, 48, 225–234.

Bogue, R.H. and Steinour, H.H. (1961) Origin of the special chemical symbols used by cement chemists. Journal of the Portland Cement Association, 3/3, 20-21.

Broekmans, M.A.T.M. (2012) Deleterious reactions of aggregate with alkalis in concrete. Reviews in Mineralogy and Geochemistry, 74, 279-364.

Burg, A., Kolodny, Ye., and Lyakhovsky, V. (1999) Hatrurim-2000: the "Mottled Zone" revisited, forty years later. Israel Journal of Earth Sciences, 48, 209–223.

Burg, A., Starinsky, A., Bartov, Y., and Kolodny, Ye. (1991) Geology of the Hatrurim Formation ("Mottled Zone") in the Hatrurim basin. Israel Journal of Earth Sciences, 40, 107–124.

Campbell, D.H. (1999) Microscopical Examination and Interpretation of Portland Cement and Clinker, second edition, 201p. Portland Cement Association, Skokie.

Church, B.N., Matheson, A., and Hora, Z.D. (1979) Combustion metamorphism in the Hat Creek area, British Columbia. Canadian Journal of Earth Sciences, 16, 1882-1887.

Cosca, M.A., and Peacor, D. (1987) Chemistry and structure of esseneite, ($CaFe^{3+}AlSiO_6$), a new pyroxene produced by pyrometamorphism. American Mineralogist, 72, 148-156.

Cosca, M.A., Essene, E.J., Geissman, J.W., Simmons, W.B., and Coates, D.A. (1989) Pyrometamorphic rocks associated with naturally burned coal beds, Powder River Basin, Wyoming. American Mineralogist, 74, 85-100.

Cuberos, A.J.M., De la Torre, A.G., Álvarez-Pinazo, G., Martín-Sedeño, M. C., Schollbach, K., Pöllmann, H., and Aranda, M.A.G. (2010) Active iron-rich belite sulfoaluminate cements: Clinkering and Hydration. Environmental Sciense and Technology, 44, 6855-6862.

De la Torre, Á.G., Cuberos, A.J.M., Álvarez-Pinazo, G., Cuesta, A., and Aranda M.A.G.

(2011) In situ powder diffraction study of belite sulfoaluminate clinkering. Journal of Synchrotron Radiation, 18, 506-514.

Deer, W.A., Howie, R.A., and Zussman, J. (1992) An introduction to the rock forming minerals. 2nd excerpted student edition, 696p. Longman, Burnt Mill.

Fleischer, M., Cabri, L.J., Chao, G.Y., and Pabst, A. (1978) New mineral names. American Mineralogist, 63, 424-427.

Fleurance, S., Cuney, M., Malartre, F., and Reyx, J. (2013) Origin of the extreme polymetallic enrichment (Cd, Cr, Mo, Ni, U, V, Zn) of the Late Cretaceous–Early Tertiary Belqa Group, central Jordan. Palaeogeography, Palaeoclimatology, Palaeoecology, 369, 201-219.

Fourcade, S., Trotignon, L., Boulvais, P., Techer, I., Elie, M., Vandamme, D., Salameh, E., and Frimmel, H.E. (2009) Trace element distribution in Neoproterozoic carbonates as palaeoenvironmental indicator. Chemical Geology, 258, 338-353.

Fukuda, K. (2001) Recent progress in crystal chemistry of belite: Intracrystalline microtextures induced by phase transformations and application of remelting reaction to improvement of hydration reactivity. Journal of the ceramic Society of Japan, 109, 43-48.

Fukuda, K. and Ando, H. (2002) Determination of the *Pcmn*/*Ibm*2 phase boundary at high temperature in the system $Ca_2Fe_2O_5$–$Ca_2Al_2O_5$, Journal of the American Ceramic Society, 85, 1300–1303.

Fukuda, K. and Maki, I. (1989) Orientation of β-Ca_2SiO_4 solid solution lamellae formed in the host α-phase. Cement and Concrete Research, 19, 913–918.

Fukuda, K. and Maki, I. (1993) Orientation of coherent interphase boundaries formed by the α to α'_H phase transition in belite crystals. Cement and Concrete Research, 23, 599–602.

Fukuda, K. and Taguchi, H. (1999) Hydration of α'_L- and β-dicalcium silicates with identical concentration of phosphorus oxide. Cement and Concrete Research, 29, 503-506.

Galuskin, E.V., Armbruster, T., Galuskina, I.O., Lazic, B., Winiarski, A., Gazeev, V.M., Dzierżanowski, P., Zadov, A.E., Pertsev, N.N., Wrzalik, R., Gurbanov, A.G., and Janeczek, J. (2011) Vorlanite $(CaU^{6+})O_4$ – A new mineral from the Upper Chegem caldera, Kabardino-Balkaria, Northern Caucasus, Russia. American Mineralogist, 96, 188-196.

Galuskin, E.V., Galuskina, I.O., Dubrovinsky, L.S., and Janeczek, J. (2012) Thermally induced transformation of vorlanite to "protovorlanite": Restoration of cation ordering in self-irradiated $CaUO_4$. American Mineralogist, 97, 1002–1004.

Galuskin, E.V., Kusz, J., Armbruster, T., Galuskina, I.O., Marzec, K., Vapnik, Ye., and Murashko, M. (2013) Vorlanite, $(CaU^{6+})O_4$, from Jabel Harmun, Palestinian Autonomy, Israel. American Mineralogist, 98, 1938-1942.

Gartner, E. (2004) Industrially interesting approaches to low-CO_2 cements. Cement and Concrete Research, 34, 1489-1498.

Gartner, E. and Li, G. (2006) High belite-containing sulfoaluminous clinker, method for the production and the use thereof for preparing hydraulic binders, Patent international application number PCT/FR2005/050595

Gilat, A. (1998) Hydrothermal activity and hydro-explosions as a cause of natural combustion and pyrolysis of bituminous rocks: the case of Pliocene metamorphism in Israel (Hatrurim Formation). Geological Survey of Israel Current Research, 11, 96-102.

Goldreich, Y. (2003) The climate of Israel, observation, research and application, 298p. Kluwer Academic/Prenum Publishers, New York.

Grapes, R. (2011) Pyrometamorphism, second edition, 290p. Springer, Berlin.

Grapes, R., Korzhova, S., Sokol, E.V. and Seryotkin, Y. (2011) Paragenesis of unusual Fe-cordierite (sekaninaite)-bearing paralava and clinker from the Kuznetsk coal basin, Siberia, Russia. Contributions to Mineralogy and Petrology, 162(2), 253-273.

Grapes, R., Sokol, E.V., Kokh, S., Kozmenko, O. and Fishman, I. (2013) Petrogenesis of Na-rich paralava formed by methane flares associated with mud volcanism, Altyn-Emel National Park, Kazakhstan. Contributions to Mineralogy and Petrology, 165, 781-803.

Grapes, R., Zhang, K., and Peng Z. (2009) Paralava and clinker products of coal combustion, Yellow River, Shanxi Province, China. Lithos, 113, 831-843.

Gross, S. (1977) The mineralogy of the Hatrurim Formation, Israel. Geological Survey of Israel Bulletin, 70, 1-80.

Gross, S. (1984) Occurrence of ye'elimite and ellestadite in an unusual cobble from the "pseudo-conglomerate" of the Hatrurim Basin, Israel. Geological Survey of Israel Current Research (1983–84), 1-4.

Gur, D., Steinitz, G., Kolodny, Y., Starinsky, A., and McWilliams, M. (1995) $^{40}Ar/^{39}Ar$

dating of combustion metamorphism ("Mottled Zone", Israel). Chemical Geology, 122, 171-184.

Hirsch, F., Burg, A., and Avni, Y. (2008) Geological Map of Israel 1:50 000, Arad, Sheet 15-IV, Jerusalem.

Humphries, D.W. (1992) The preparation of thin sections of rocks, minerals and ceramics. p83. Royal Microscopical Society, Oxford Science Publications, Microscopy Handbooks (24).

Idrissi M., Diouri, A. Damidot, D., Greneche, J.M., Alami Talbi, M., and Taibi, M. (2010) Characterisation of iron inclusion during the formation of calcium sulfoaluminate phase. Cement and Concrete Research, 40, 1314-1319.

Idrissi, M., Diouri, A., Alami Talbi, M., Sassi, O., and Damidot, D. (2012) Hydration behavior of iron doped calcium sulfoaluminate phase at room temperature. MATEC Web of Conferences, Volume 2, IInd International Seminar Innovation & Valorization in Civil Engineering & Construction Materials, DOI: http://dx.doi.org/10.1051/matecconf/20120201005

Justnes, H. (2012) Alternative low-CO_2 'green' clinkering. Reviews in Mineralogy and Geochemistry, 74, 83-99.

Khoury, H. (2007) Cementation of kerogen-rich marls by alkaline fluids released during weathering of thermally metamorphosed marly sediments. Part I: Isotopic (C, O) study of the Khushaym Matruk natural analogue (Central Jordan). Applied Geochemistry, 22, 1293-1310.

Khoury, H. and Nassir, N. (1982) High temperature mineralization in Maqarin area, North Jordan. Neues Jahrbuch für Mineralogie (Abhandlungen), 144, 197-213.

Khoury, H.N. and Milodowski, T.E. (1992) High temperature metamorphism and low temperature retrograde alteration of spontaneously combusted marls. The Maqarin cement analogue, Jordan, p. 1515-1518 in: Proceedings of the 7th Symposium on Water-Rock Interaction, Park City, Utah, 13-18 July 1992.

Kokh, S.N. (2010) Ye'elimite and fluorellestadite as new indicators of ultrahigh-temperature–ambient pressure metamorphism in: IMA2010; 20th General Meeting of the International Mineralogical Association; abstracts. Acta Miner.-Petrograph., Abstract Series, 6, 521.

Kolodny, Y. (1979) Natural cement factory: a geological story, in: J. Skalny (Ed.). Cement Production and Use. Franklin Pierce College, Rindge, New Hampshire, 203–216.

Kolodny, Y. and Gross, S. (1974) Thermal metamorphism by combustion of organic matter: isotopic and petrological evidence. Journal of Geology, 82, 489-506.

Maki, I. (1994) Processing conditions of Portland cement clinker as viewed from the fine textures of the constituent minerals. Ceramic Transactions, 40, 3-17.

Marinho, M.B. and Glasser, F.P. (1984) Polymorphism and phase changes in the ferrite phase of cements induced by titanium substitution. Cement and Concrete Research, 14, 360-368.

Martín-Sedeño, M. C., Cuberos, A.J.M., De la Torre, Á.G., Álvarez-Pinazo, G., Ordónez, L.M., Gateshki, M., and Aranda, M.A.G. (2010) Aluminum-rich belite sulfoaluminate

cements: Clinkering and early age hydration. Cement and Concrete Research, 40, 359-369.

Matthews, A. and Gross, S. (1980) Petrologic evolution of the "Mottled Zone" (Hatrurim) metamorphic complex of Israel. Israel Journal of Earth Sciences, 29, 93–106.

Mehta, P.K. (1978) Energy resources in the environment – a review of the US cement industry. World Cement Technology, 9, 144-160.

Mehta, P.K. (1980) Investigations on energy-saving cements. World Cement Technology, 11, 166-177.

Morgan, G.B. and London, D. (2005) Effect of current density on the electron microprobe analysis of alkali aluminosilicate glasses. American Mineralogist, 90, 1131-1138.

Ono, Y. (1980a) Microscopical test of clinker and its background, Journal of Research, Onoda Cement Company, 32 (104), 101-109.

Ono, Y. (1980b) Microscopy for the quality control of cement, Journal of Research,Onoda Cement Company, 32 (104), 110-112.

Othmane, G., Allard, Th., Menguy, N., Morin, G., Esteve, I., Fayek, M., and Calas, G. (2013) Evidence for nanocrystals of vorlanite, a rare uranate mineral, in the Nopal I low-temperature uranium deposit (Sierra Peña Blanca, Mexico). American Mineralogist, 98, 518-521.

Papike, J.J. (1987) Chemistry of the rock-forming silicates: Ortho, ring, and single-chain structures. Reviews of Geophysics, 25(7), 1483-1526.

Papike, J.J. (1988) Chemistry of the rock-for ming silicates: Multiple-chain, sheet, and framework structures. Reviews of Geophysics, 26(3), 407-444.

Phedorin, M.A., Bobrov, V.A., Chebykin, E.P., Goldberg, E.L., Melgunov, M.S., Filippova, S.V., and Zolotarev, K.V. (2000) Comparison of synchrotron radiation X-ray fluorescence with conventional techniques for the analysis of sedimentary samples. Journal of Geostandards and Geolanalysis, 24, 205-216.

Pöllmann, H. (2010) Mineralisation of wastes and industrial residues, 478p. Shaker Verlag, Aachen/DE.

Pöllmann, H. (2012) Calcium aluminate cement – raw materials, differences, hydration, and properties. Reviews in Mineralogy and Geochemistry, 74, 1-82.

Quillin, K. (2001) Performance of belite–sulfoaluminate cements. Cement and Concrete Research, 9, 1341-1349.

Redhammer, G. J., Tippelt, G., Roth, G., and Amthauer, G. (2004) Structural variations in the brownmillerite series $Ca_2(Fe_{2-x}Al_x)O_5$: Single-crystal X-ray diffraction at 25° C and high-temperature X-ray powder diffraction (25° C ≤ T ≤ 1000° C). American Mineralogist, 89, 405-420.

Reverdatto, V.V. (1973) The facies of contact metamorphism, translated in English from Russian, 263p. Australian National University, Canberra.

Senff, L., Castela, A., Hajjaji, W., Hotza, D., and Labrincha J.A. (2011) Formulations of sulfobelite cement through design of experiments. Construction and Building Materials, 25, 3410-3416.

Seryotkin, Yu.V., Sokol, E.V., and Kokh, S.N. (2012) Natural pseudowollastonite: crystal structure, associated minerals, and geological context. Lithos, 133-135, 75-90.

Sharygin, V.V. (2012) Mineralogy of metacarbonate xenolith from alkali basalt, E. Eifel, Germany, in: Ore Potential of Alkaline, Kimberlite and Carbonatite Magmatism. Book of Abstracts, XXIX International Conference. Training Program: Alkaline Magmatism of the Earth, Sudak-Moscow, ONTI GEOCHI RAS, 156-158.

Sharygin, V.V., Lazic, B., Armbruster, T.M., Murashko, M.N., Wirth R., Galuskina, I., Galuskin, E.V, Vapnik, Ye., Britvin, N., and Logvinova, A.M. (2013) Shulamitite $Ca_3TiFe^{3+}AlO_8$ – a new perovskite-related mineral from Hatrurim Basin, Israel. European Journal of Mineralogy, 25, 97-111.

Sharygin, V.V., Sokol, E.V., and Vapnik, Ye. (2008) Minerals of the pseudobinary perovskite-brownmillerite series from combustion metamorphic larnite rocks of the Hatrurim Formation (Israel). Russian Geology and Geophysics, 49 (10), 709-726.

Shatsky, V.S., Sitnikova, E.S., Koz'menko, O.A., Palessky, S.V., Nikolaeva, I.V., and Zayachkovsky, A.A. (2006) Behavior of incompatible elements during ultrahigh-pressure metamorphism (by the example of rocks of the Kokchetav massif). Russian Geology and Geophysics, 47, 482-496.

Sokol, E.V., Maksimova, N.V., Nigmatulina, E.N., Sharygin, V.V., and Kalugin, V.M. (2005) Combustion Metamorphism, 284p. Publishing house of the Siberian Branch of the Russian Academy of Science, Novosibirsk. In Russian.

Sokol, E.V., Novikov, I.V., Zateeva, S.N., Sharygin, V.V., and Vapnik, Ye. (2008) Pyrometamorphic rocks of the spurrite-merwinite facies as indicators of hydrocarbon discharge zones (the Hatrurim Formation, Israel). Doklady Earth Sciences, 420, 608–

614.

Sokol, E.V., Novikov, I.V., Zateeva, S.N., Vapnik, Ye., Shagam, R., and Kozmenko, O.A.; (2010) Combustion metamorphic rocks as indicators of fossil mud volcanism: New implications for the origin of the Mottled Zone, Dead Sea rift area. Basin Research, 22, 414–438.

Sokol, E.V., Gaskova, O.L., Kokh, S.N., Kozmenko, O.A., Seryotkin, Yu.V., Vapnik, Ye., and Murashko, M.N. (2011) Chromatite and its Cr^{3+}- and Cr^{6+}-bearing precursor minerals from the Nabi Musa Mottled Zone complex, Judean Desert. American Mineralogist, 96, 659-674.

Sokol, E.V., Kozmenko, O.A., Kokh, S.N., and Vapnik, Ye. (2012) Gas reservoirs in the Dead Sea area: evidence from chemistry of combustion metamorphic rocks in Nabi Musa fossil mud volcano, Russian Geology and Geophysics, 53, 745-762.

Stöber, S., Redhammer, G., Schorr, S., Prokhnenko, O., and Pöllmann, H. (2013) Structure refinements of members in the brownmillerite solid solution series $Ca_2Al_x(Fe_{0.5}Mn_{0.5})_{2x}O_{5+\delta}$ with $½ \leq x \leq 4/3$. Journal of Solid State Chemistry, 197, 420–428.

Taylor, H.F.W. (1997) Cement Chemistry, second edition, 459p. Thomas Telford Services, London.

Techer, I., Khoury, H.N., Salameh, E., Rassineux, F., Claude, C., Clauer, N., Pagel, M., Lancelot, J., Hamelin, B., and Jacquot., E. (2006) Propagation of high-alkaline fluids in an argillaceous formation: Case study of the Khushaym Matruk natural analogue (Central Jordan). Journal of Geochemical Exploration, 90, 53–67.

Vapnik, Ye. and Vardi, J. (2013) Combustion metamorphic stone tools, Hatrurim basin, Israel. In: G.B. Stracher, A. Prakash, E.V. Sokol (Eds.). Coal and Peat Fires: A Global Perspective. Vol. 2: Photographs and Multimedia Tours, Elsevier, Amsterdam, 189-201.

Vapnik, Ye., Sharygin, V.V., Sokol, E.V., and Shagam, R. (2007) Paralavas in combustion metamorphic complex at the Hatrurim Basin, Israel. In: G. Stracher (Ed.), Geology of Coal Fires: Case Studies from Around the World, Geological Society of America, Reviews in Engineering Geology, XVIII, 133-153.

Vardi, J. and Cohen-Sasson, E. (2012) Har-Parsa: a large-scale larnite quarry and bifacial tool production site in the Judean Desert, Israel. Antiquity, 086 (332).

Yamnova, N.A., Zubkova, N.V., Eremin, N.N., Zadov, A.E., and Gazeev, V.M. (2011) Crystal structure of larnite β - Ca_2SiO_4 and specific features of polymorphic transitions in dicalcium orthosilicate. Crystallography Reports, 56(2), 210-220.

Zateeva, S.N., Sokol, E.V., and Sharygin, V.V. (2007) Specificity of pyrometamorphic minerals of the ellestadite group. Geology of Ore Deposits, 49, 8, 792–805.

Zenin, V.N. (2012) Archaeological sites in areas of mud volcanism, in: Problems of Archaeology, Ethnography, and Anthropology of Siberia and Adjacent Territories. Proceedings of the Annual Session of the Institute of Archaeology and Ethnography, Volume XVIII, Novosibirsk, 83-87. (in Russian).

Zhang, L., Su, M., and Wang, Y. (1999) Development of the use of sulfo- and ferroaluminate cements in China. Advances in Cement Research, 11, 15-21.

Zhang, X., Zhao, M., and Zhang, Y. (2012) Preparation and properties of self-pulverizing sulfoaluminate cement. Construction and Building Materials, 34, 107-113.

Zvereva V.V. (2009) SR XRF Analysis of Cardiac and Vascular Tissues in Humans: Approaches and Methods. PhD Thesis in Chemistry. Novosibirsk, 131 pp. (in Russian).

Figure captions

Fig. 1. Location map of the Dead Sea Transform area, modified after Sokol et al. (2010), showing outcrops of the Mottled Zone near the Dead Sea (a). Generalized geological map of the Hatrurim Basin (b). Geology simplified after 1:200000 Geological Map of Israel (Sneh et al. 1998) and (Burg et al. 1991).

Fig 2. Larnite-bearing rocks from Hatrurim Basin.
(a) Typical larnitic rocks that have undergone marginal hydration and carbonation, to produce so-called pseudo conglomerate; (b) massive fresh larnite (and ye'elimite-larnite) rocks making up blocks, slabs or cliffed hilltops; (c) weathering forms of ye'elimite-larnite rocks at Har-Parsa; "balls" of fresh ye'elimite-larnite rocks coated with calcite, ettringite, and gypsum.

Fig. 3. Selected examples of XRPD diffractograms for ye'elimite-larnite rocks in samples YV410-413. Bulk Co Kα radiation (1.78 Å), characteristic peaks labeled cf. ICDD numbers.

Fig. 4. Paleolithic stone tool factory on the flat top of Har-Parsa.

(a) Panoramic view of the Har-Parsa eastern slope; at the back: a cliff-like outcrop of larnitic rocks; in the front: a flat surface where stone tools were fabricated, with stacks of blanks, chips, and half-finished tools (see hammer as a scale among the YL rock debris); (b) typical Prehistoric bifacial stone tools with weak surface abrasion made from ye'elimite-larnite rocks; (c) man-made breccia composed of ye'elimite-larnite rock gallets and cemented by secondary calcite (sample YV - 413).

Fig. 5. Photomicrographs of ye'elimite-larnite rocks and elemental (Ca, Si, Al, S, P, Fe, Ti, Na) maps. Sample YV-413. *Ap* = fluorapatite, *Brm* = brownmillerite, *Lrn* = larnite, *Shu* = Fe-analogue of shulamitite, *Yel* = ye'elimite.

Fig. 6. Ye'elimite-larnite rocks. General view.
a, c: Photomicrographs in polarised transmitted light showing uniformly distributed rock-forming minerals (a) and a large fluorellestadite (*Els*) crystal crowded with inclusions of ye'elimite (*Yel*) and brownmillerite *(Brm)*; b, d: BSE images. Other abbreviations as in Fig. 4.

Fig. 7. Two sets of intersecting lamellae in a natural α′ - Ca_2SiO_4 polymorph indicating its affinity to a natural equivalent of type I belite. SEM image. Sample YV - 413.

Fig. 8. (a) and (b) Optical photomicrograph of belite from an industrial clinker, showing the so-called "striation", as termed in the cement industry, consisting of several sets of lamellae intersecting each other. Transmitted plane-polarized light.

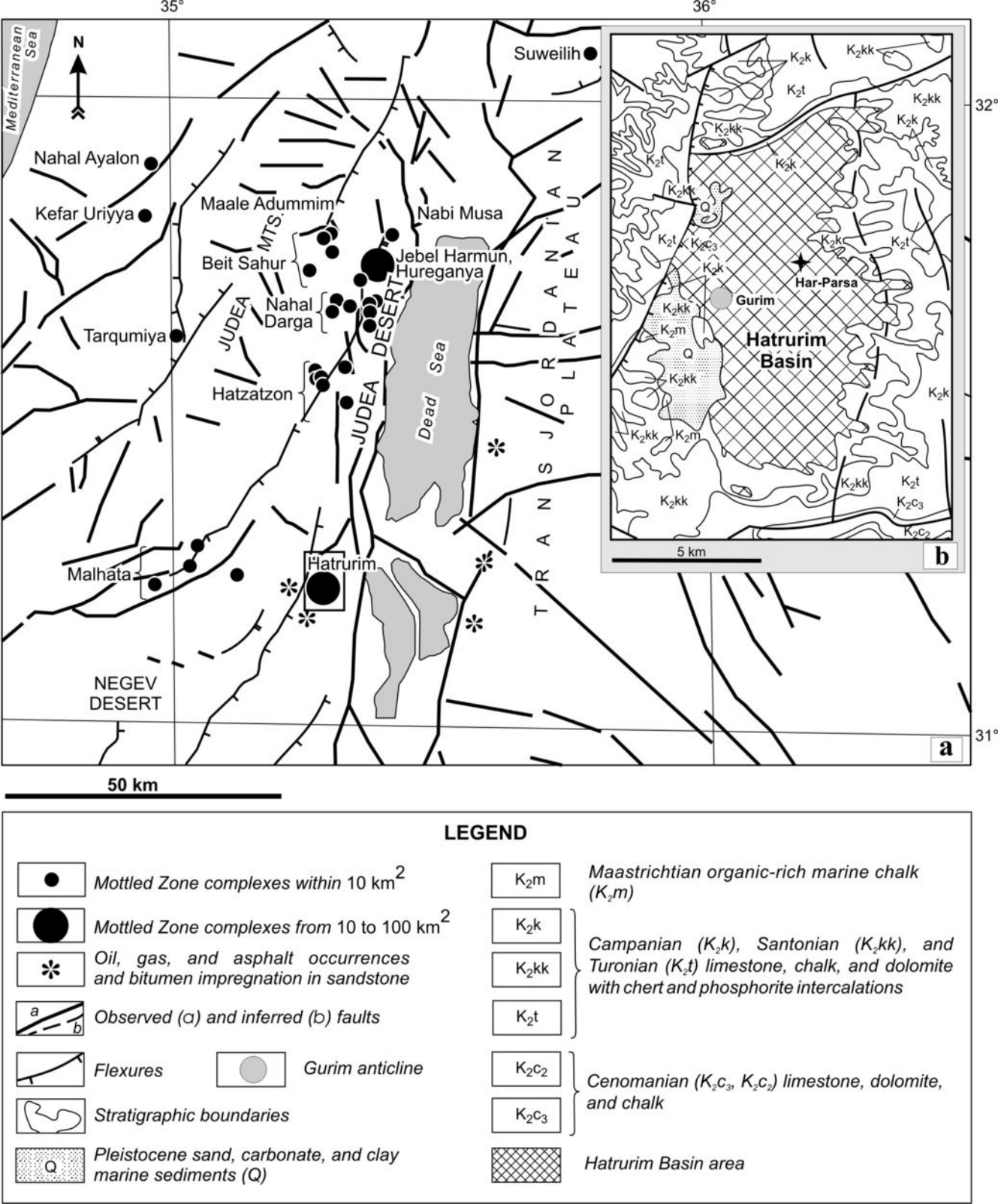
35°
36°
32°
31°
Mediterranean Sea
N
Suweilih
Nahal Ayalon
Kefar Uriyya
Maale Adummim
Nabi Musa
Beit Sahur
Jebel Harmun, Hureganya
Nahal Darga
Tarqumiya
Hatzatzon
Dead Sea
Malhata
Hatrurim
NEGEV DESERT
JUDEA MTS.
JUDEA DESERT
TRANSJORDANIAN PLATEAU
50 km
a
K2k
K2kk
K2t
K2c3
K2c2
K2m
Q
Har-Parsa
Gurim
Hatrurim Basin
5 km
b
LEGEND
Mottled Zone complexes within 10 km2
Mottled Zone complexes from 10 to 100 km2
Oil, gas, and asphalt occurrences and bitumen impregnation in sandstone
Observed (a) and inferred (b) faults
Flexures
Gurim anticline
Stratigraphic boundaries
Pleistocene sand, carbonate, and clay marine sediments (Q)
Maastrichtian organic-rich marine chalk (K2m)
Campanian (K2k), Santonian (K2kk), and Turonian (K2t) limestone, chalk, and dolomite with chert and phosphorite intercalations
Cenomanian (K2c3, K2c2) limestone, dolomite, and chalk
Hatrurim Basin area


a
1.5 cm


b


c

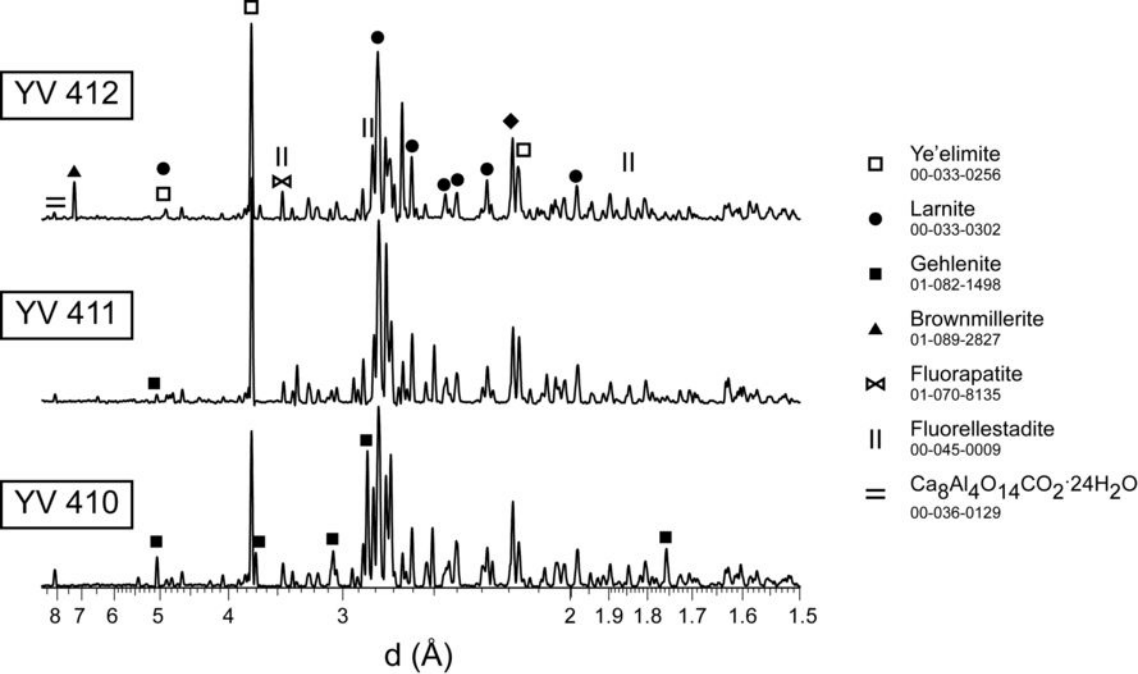
YV 412
YV 411
YV 410
8 7 6 5 4 3 2 1.9 1.8 1.7 1.6 1.5
d (Å)
Ye'elimite
00-033-0256
Larnite
00-033-0302
Gehlenite
01-082-1498
Brownmillerite
01-089-2827
Fluorapatite
01-070-8135
Fluorellestadite
00-045-0009
$Ca_8Al_4O_{14}CO_2 \cdot 24H_2O$
00-036-0129

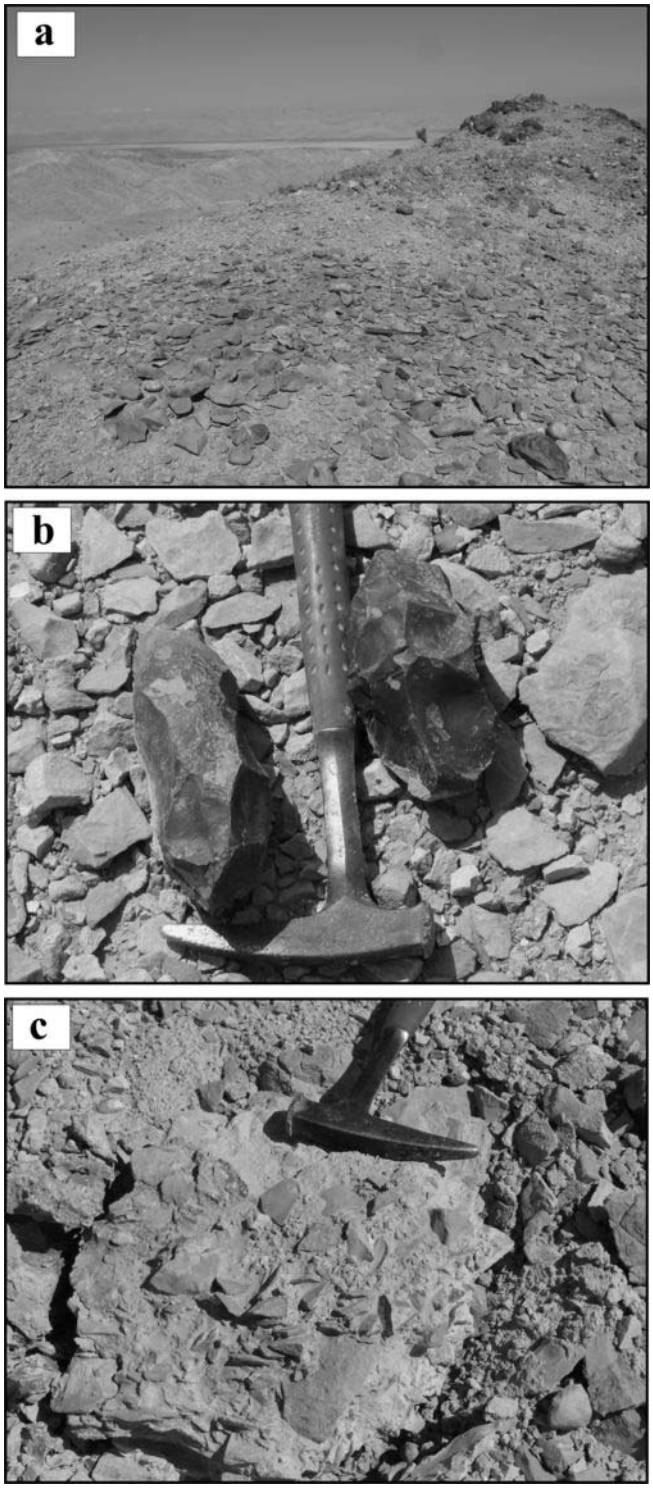
a
b
c

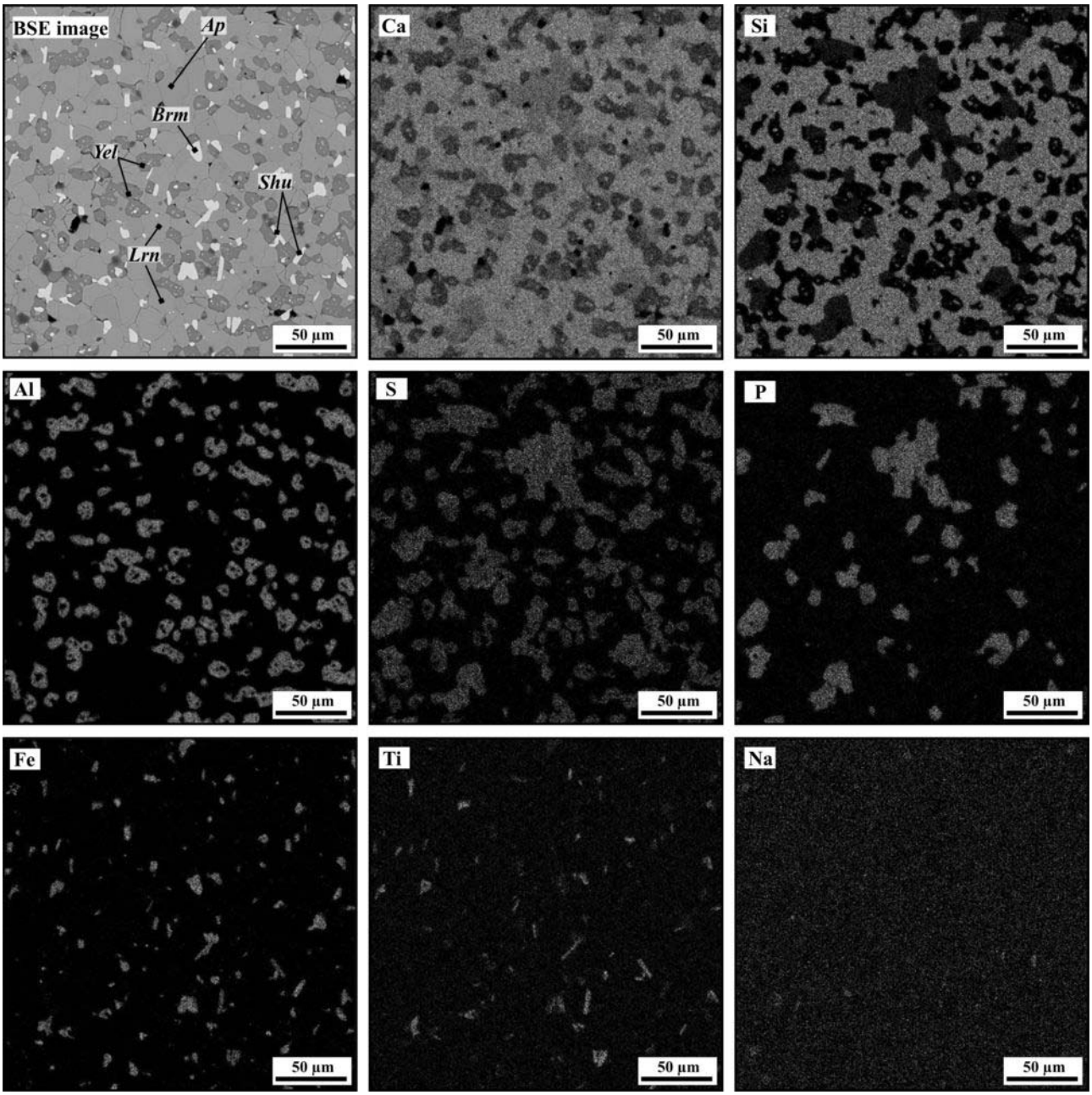
BSE image
Ap
Brm
Yel
Shu
Lrn
50 µm
Ca
Si
Al
S
P
Fe
Ti
Na

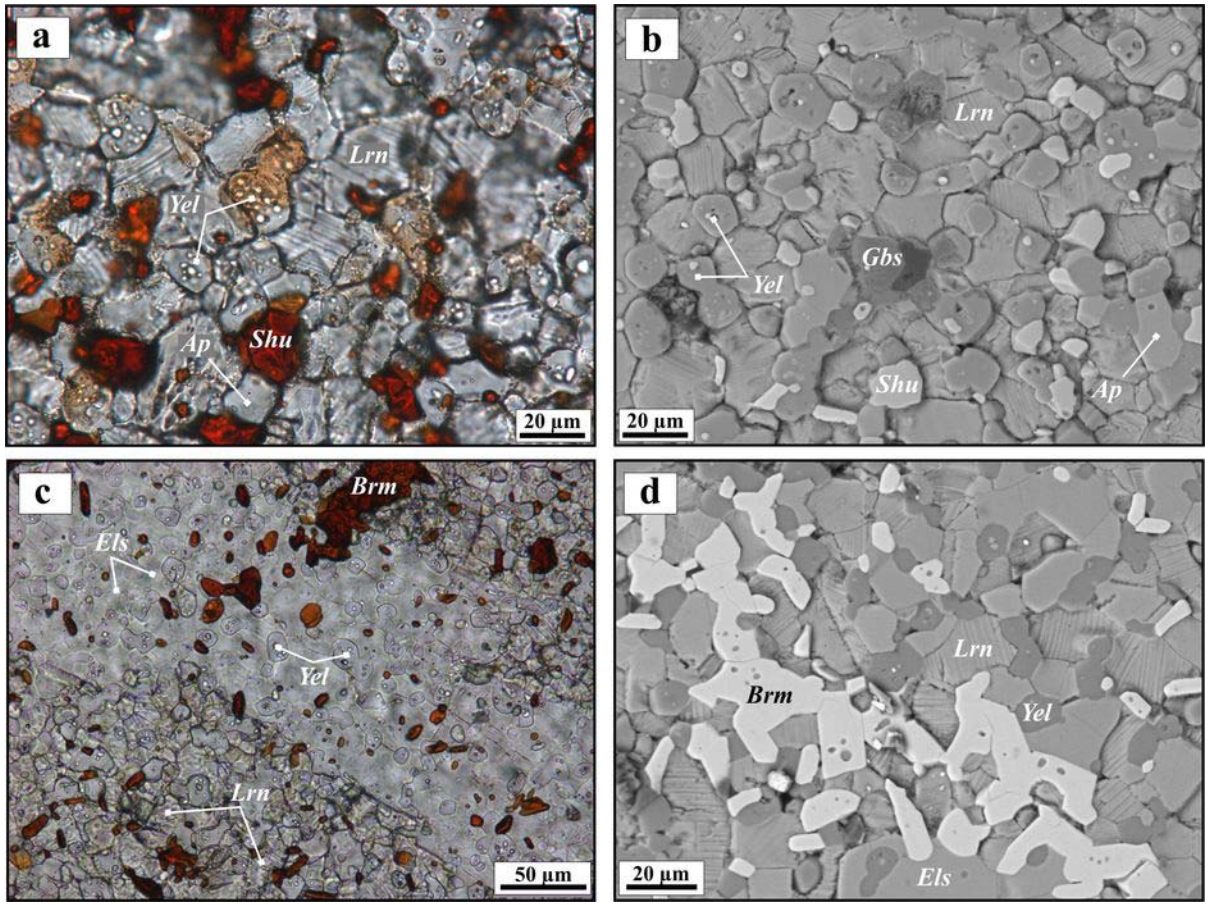
a
Lrn
Yel
Ap
Shu
20 µm
b
Lrn
Gbs
Yel
Shu
Ap
20 µm
c
Brm
Els
Yel
Lrn
50 µm
d
Lrn
Brm
Yel
Els
20 µm

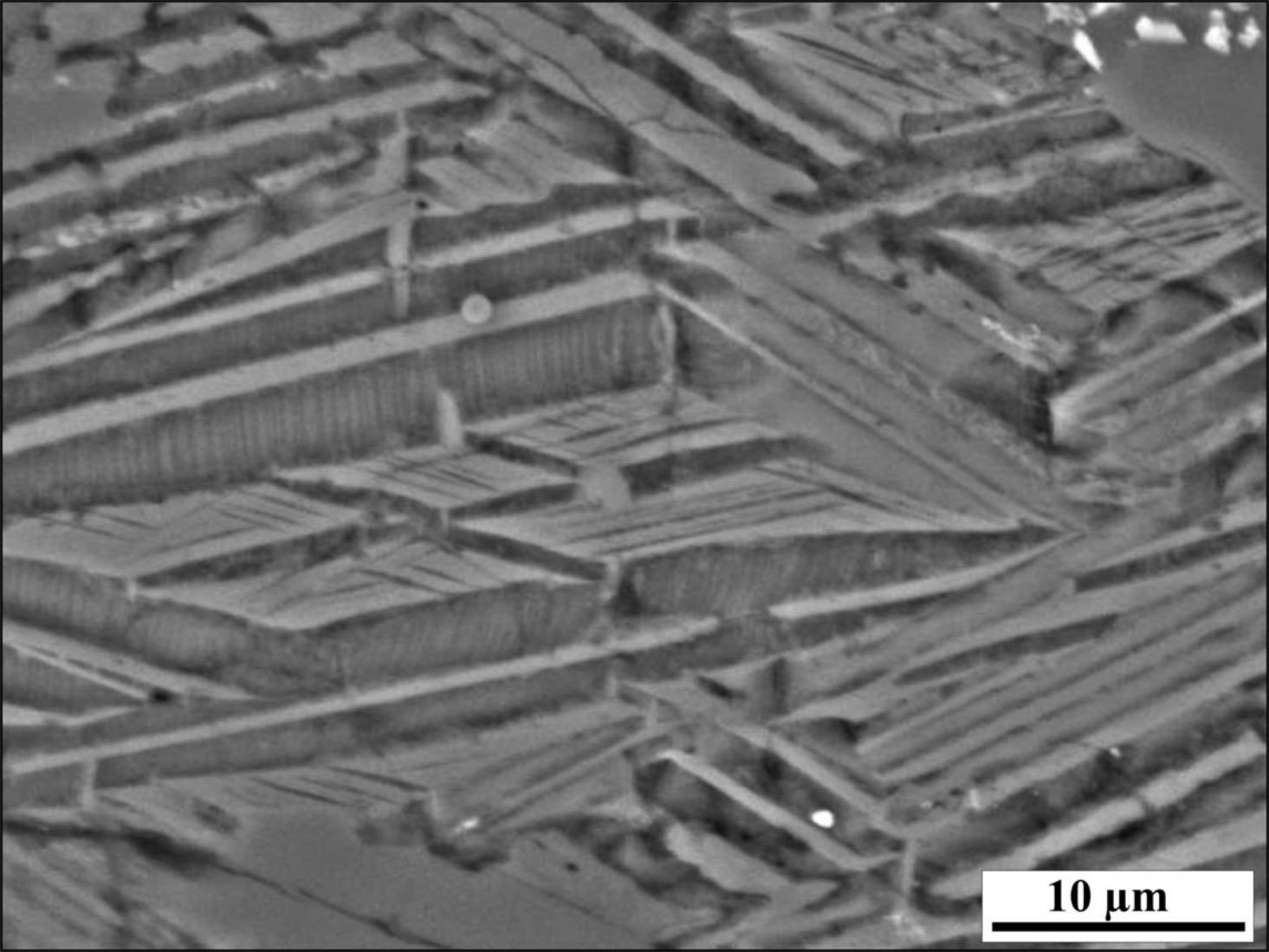
10 µm

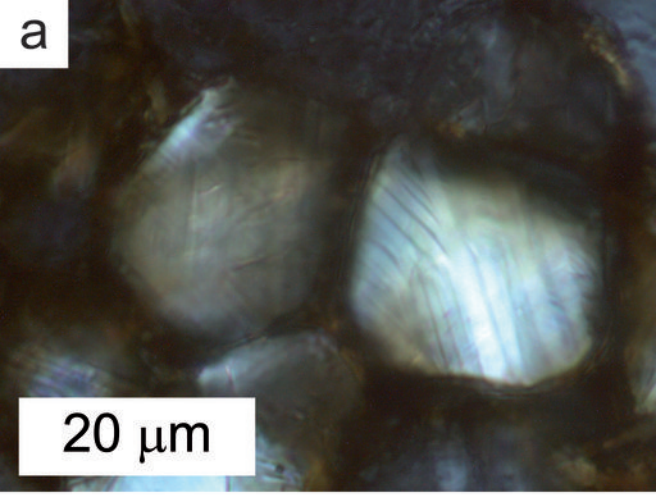
a
20 μm

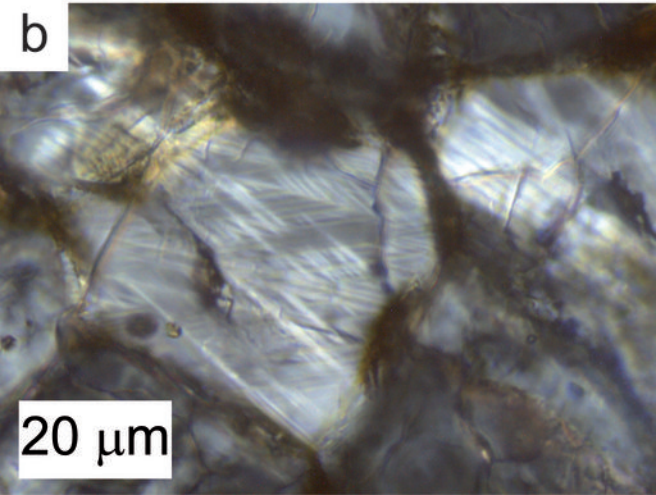
b
20 μm

Table 1. Minerals occurring in the Ca-rich combustion metamorphic rocks of the Hatrurim Formation in Israel, and their CAS notations

Mineral	Chemical formula	Symmetry	CAS notation
Silicates			
Hatrurite	Ca_3SiO_5	trigonal	C_3S (Alite)
α'-Ca_2SiO_4 (unnamed)	α'-Ca_2SiO_4	orthorhombic	C_2S (Type I belite)
Larnite	β-Ca_2SiO_4	monoclinic	C_2S (Type II belite)
Calcioolivine	γ-Ca_2SiO_4	orthorhombic	γ-Ca_2SiO_4
Rankinite	$Ca_3Si_2O_7$	monoclinic	C_3S_2
Pseudowollastonite	α-$Ca_3Si_3O_9$	monoclinic	α-CS
Wollastonite	β-$Ca_3Si_3O_9$	triclinic	β-CS
Parawollastonite	$Ca_3Si_3O_9$	monoclinic	CS
Bredigite	$Ca_7Mg(SiO_4)_4$	orthorhombic	C_7MS_4
Merwinite	$Ca_3Mg(SiO_4)_2$	monoclinic	C_3MS_2
Monticellite	$CaMgSiO_4$	orthorhombic	CMS
Gehlenite	$Ca_2Al_2SiO_7$	tetragonal	C_2AS
Polyanionic minerals			
Nagelschmidtite[a]	$Ca_7Si_2P_2O_{16}$	hexagonal	$C_7S_2P_2$
Spurrite	$Ca_5(SiO_4)_2(CO_3)$	monoclinic	$C_5S_2\overline{C}$
Ye'elimite[b]	$Ca_4Al_6O_{12}(SO_4)$	isometric, tetragonal, orthorhombic	$C_4A_3\overline{S}$
Cuspidine	$Ca_4(Si_2O_7)F_2$	monoclinic	$C_4S_2\overline{F}_2$
Fluorapatite	$Ca_{10}(PO_4)_6F_2$	hexagonal	$C_{10}P_6\overline{F}_2$
Fluorellestadite	$Ca_{10}[(SiO_4),(PO_4),(SO_4)]_6F_2$	hexagonal	$C_{10}S_3\overline{S}_3\overline{F}_2$
Fluormayenite	$Ca_{12}Al_{14}O_{32}[(H_2O)_nF_2]$	isometric	$C_{12}A_7H_n\overline{F}_2$
Aluminate			
Grossite	$CaAl_4O_7$	monoclinic	CA_2
Multiple oxides			
Brownmillerite	$Ca_2(Fe_{2-x}Al_x)O_5$	orthorhombic	C_4AF
Shulamitite[c]	$Ca_3TiFe^{3+}AlO_8$	orthorhombic	C_3FTA
Fe-analogue of shulamitite[c]	$Ca_3Fe_2TiO_8$	orthorhombic	C_3FT
Perovskite	$CaTiO_3$	orthorhombic	CT
Magnesioferrite	$MgFe^{3+}{}_2O_4$	isometric	MF
Spinel	$(Mg,Fe)Al_2O_4$	isometric	MA
Simple oxide			
Periclase	MgO	isometric	M

Notes: [a] nagelschmidtite formula according (Taylor 1997); [b] symmetry of $Ca_4Al_6O_{12}(SO_4)$ polymorphic modifications according (Idrissi et al. 2010); [c] description of Fe-analogue of shulamitite is given in (Sharygin et al. 2013). CAS notation for Fe-analogue of shulamitite cf. Stöber et al. (2013), all other notations cf. Bogue and Steinour (1961) and Pöllman (2012).

Table 2. Mineral assemblages of ye'elemite-larnite combustion metamorphic rocks, Hatrurim Basin complex

Sample/ Rock type	Main phases	Minor and *accessory* phases	Alteration products	Locality
YV-410 Gehlenite-larnite hornfels	Gehlenite, Larnite, Fluorapatite, Brownmillerite	Ye'elimite, *Hatrurite (alite)* *Fe-analog of shulamitite* *Magnesioferrite, Pyrrhotite*	*$Al(OH)_3$* after ye'elimite, *Tobermorite (tr)*	Paleolithic "factory" on the eastern slope of Har-Parsa.
YV-411 Ye'elimite-larnite rock	Larnite, Ye'elimite, Fluorapatite	Magnesioferrite *Fe-analog of shulamitite* *Magnesioferrite, Barite*	*Gibbsite* after ye'elimite, *Tobermorite (tr)*	Paleolithic "factory" on the eastern slope of Har-Parsa.
YV-412 Brownmillerite-ye'elimite-larnite rock	Larnite, Ye'elimite, Fluorellestadite, Brownmillerite	*Periclase (Fe, Ni, Zn),* *Berzelianite or bellidoite,* *Eucairite,* *Vorlanite*	*Gibbsite* after ye'elimite	Cliff-like outcrop LY rock located near top of Har-Parsa.
YV-413 The sample is man-made breccias composed of ye'elimite-larnite rock artifacts.	Larnite, Ye'elimite, Fluorapatite, Fluorellestadite, Brownmillerite	Magnesioferrite *Fe-analog of shulamitite* *α'-Ca_2SiO_4*	Calcite after larnite	Paleolithic "factory" on the eastern slope of Har-Parsa
M4-218 Shulamitite- mayenite-larnite rock (Sharygin et al. 2008, 2013).	Larnite, Mayenite (F), Shulamitite	Fluorapatite Ye'elimite, Magnesioferrite *Cr-bearing spinel,* *K-Fe sulfide (Cu,Ni-rich)*	Hillebrandite, Afwillite, Katoite, *Fashagite, Pornlandite,* *Hematite*	Isolated cobble from pseudo-conglomerate. Western Hatrurim Basin.
M5-31 Ye'elimite-larnite rock (Sharygin et al. 2008)	Larnite, Ye'elimite, Brownmillerite	Ellestadite *Fe-analog of shulamitite* Cr-bearing spinel		Isolated cobble from pseudo-conglomerate. Western Hatrurim Basin.
M5-30 Ye'elimite-larnite rock (Sharygin et al. 2008)	Larnite, Ye'elimite,	Ellestadite		Isolated cobble from pseudo-conglomerate. Western Hatrurim Basin.
H-201 Ye'elimite-larnite rock (Sharygin et al. 2008)	Larnite, Ye'elimite, Brownmillerite Fe-Mg spinel	Fluorellestadite *Fe-analog of shulamitite* Magnesioferrite		Isolated cobble from pseudo-conglomerate. Western Hatrurim Basin.
M4-217 Brownmillerite-ye'elimite-larnite rock (Sharygin et al. 2008)	Larnite, Ye'elimite, Brownmillerite	Fluorellestadite		Isolated cobble from pseudo-conglomerate. Western Hatrurim Basin.
Brownmillerite-ye'elimite-larnite rock (Gross 1984)	Larnite, Ye'elimite, Fluorapatite-Fluorellestadite$_{ss}$ Brownmillerite		Aragonite, Calcite, Vaterite, Gypsum, Ca-Al- and Ca-Si-hydrates, Portlandite, Ettringite, Halite, *Xanotlite, Clays*	Cobbles from pseudo-conglomerate exposed along Arad-Sedom road and the nearby wadies, southeastern Hatrurim Basin.
Brownmillerite-ye'elimite-larnite rock (Gross 1984)	Larnite Brownmillerite Fluorellestadite Ye'elimite		Aragonite, *Calcite, Gypsum,* *Ca-Al-hydrates,* *Halite*	Cobble (~ 15 cm in diameter) from pseudo-conglomerates, southeastern Hatrurim Basin.

Notes: Main phases (> 10 vol%), minor phases (5-10 vol%) and *accessories* (< 3 vol%).

Table 3. Bulk compositions of natural ye'elimite-larnite rocks and industrial belite-based calcium sulfoaluminate clinkers, compared (wt%)

Rock		Larnite-ye'elimite rock						BSA clinker		
Number		1	2	3	4	5	6	7	8	9
Sample	LLD	M4-217	M5-30	M5-31	YV-411	YV-412	YV-410			
SiO_2	0.25	25.9	24.6	25.6	21.9	21.0	23.0	15.0-25.0	15.0-25.0	16.5-17.6
TiO_2	0.10	0.38	0.39	0.43	0.41	0.41	0.42	–	≤ 3.00	0.30-0.40
Al_2O_3	0.25	11.7	11.7	12.1	10.4	9.88	11.9	9.00-22.0	9.00-22.0	15.8-16.9
Fe_2O_3	0.20	4.49	4.55	5.81	5.00	4.32	4.80	3.00-11.0	3.00-11.0	6.90-7.80
FeO	0.20	n.a.	n.a.	n.a.	b.d.	b.d.	b.d.	–	–	–
MnO	0.01	0.15	0.14	0.14	0.05	b.d.	0.26	–	–	–
MgO	0.20	0.93	0.82	0.82	1.37	0.81	1.13	–	1.00-4.00	0.20
CaO	0.25	51.9	52.6	50.8	53.0	56.0	51.1	50.0-61.0	50.0-61.0	50.1-52.5
Na_2O	0.05	0.30	0.15	0.72	0.47	0.25	0.18	0.20-1.00	0.10-2.00	0.10-0.70
K_2O	0.05	0.45	0.09	0.48	0.35	0.13	2.43	0.20-1.00	0.10-2.00	0.10-1.10
P_2O_5	0.03	2.25	2.31	2.07	1.92	1.34	1.82	–	≤ 4.00	0.00-1.00
S^{2-}	0.05	b.d.	b.d.	b.d.	<0.10	0.14	<0.10	–	–	–
SO_3	0.05	1.35	2.20	1.39	3.29	4.97	2.17	–	4.00-8.00	4.30-6.10
CO_2	0.06	0.62	0.89	0.08	0.86	0.76	0.49	–	–	–
B_2O_3	n.a	n.a.	n.a.	n.a.	n.a.	n.a.	n.a.	0.20-2.00	≤ 2.00	0.00-1.40
H_2O^+	0.05	n.a.	n.a.	n.a.	0.22	0.10	0.10	–	–	–
Total	–	100.4	100.4	100.4	99.2	100.1	99.8	–	–	–

Note: 1-6 = ye'elimite-larnite rocks, Hatrurim Basin complex, Israel (see Table 2 for details); 7-9 = compositions of belite-based calcium sulfoaluminate clinkers (according to Gartner and Li (2006)); 7 = range of optimal compositions (additional doping components CaF_2 and $CaCl_2$ up to 1 wt%); 8 = range of preferable compositions (additional doping components CaF_2 and $CaCl_2$ up to 3 wt%); 9 = range of experimental compositions; b.d. = below detection; n.a. = not analyzed.

Table 4. Trace-element composition of ye'elimite-larnite rocks (ppm)

Sample	LLD	M4-217	M5-30	M5-31	YV-410	YV-411	YV-412
V	2.0	49	40	53	82	112	40
Cr	1.5	95	182	377	175	243	224
Ni	1.0	129	152	205	214	151	240
Cu	1.0	35	103	66	40	58	96
Zn	1.0	249	59	426	333	343	244
Ga	0.7	8	9	9	12	9	8
Ge	0.2	2	2	1	3	1	1
Se	0.2	23	b.d.	b.d.	b.d.	10	96
Rb	0.2	12	3	10	3	8	5
Sr	1.0	2203	2903	2050	1407	1502	2009
Y	0.2	69	35	35	53	52	37
Zr	0.5	77	69	80	69	67	69
Nb	0.2	11	6	8	10	9	9
Mo	0.2	7	9	19	3	10	16
As	0.8	9	22	13	19	15	13
Sb	1.0	1	b.d.	2	b.d.	b.d.	b.d.
Ba	1.0	128	24	441	1459	2010	451
La	2.0	50	26	21	n.a.	n.a.	n.a.
Ce	1.0	42	32	28	n.a.	n.a.	n.a.
Pb	0.8	3	b.d.	9	9	47	19
Th	1.0	8	b.d.	12	9	9	11
U	1.0	2	b.d.	27	14	26	24

Notes: b.d. = below detection; n.a. = not analyzed; Ag Cd In Sn Te I Cs ≤1 ppm.

Table 5. Composition of larnite and α'-Ca_2SiO_4 modification (wt%)

Sample		YV-411				YV-412				YV-413									Ca_2SiO_4 theor.
Phase	LLD	Larnite			average n=19	Larnite			average n=20	Larnite				average n=7	α'-Ca_2SiO_4			average n=4	
SiO_2	0.03	33.5	33.6	34.1	33.5	32.9	33.0	33.5	33.2	33.5	32.8	33.9	34.4	33.8	34.2	34.5	34.2	34.3	34.9
TiO_2	0.02	0.08	0.10	0.06	0.07	0.08	0.08	0.08	0.07	0.39	0.08	0.07	0.05	0.12	0.06	0.05	0.08	0.06	
Al_2O_3	0.02	0.12	0.13	0.08	0.12	0.18	0.21	0.27	0.29	0.30	0.27	0.21	0.04	0.19	0.66	0.04	0.06	0.25	
FeO-total	0.02	0.13	0.29	0.12	0.14	0.10	0.20	0.13	0.13	0.41	0.07	0.11	b.d.	0.17	0.08	0.02	0.05	0.05	
MgO	0.02	b.d.	b.d.	b.d.	b.d.	b.d.	b.d.	b.d.	b.d.	0.08	0.08	0.31	0.06	0.12	0.10	0.04	0.03	0.06	
V_2O_5	0.03	0.04	0.05	b.d.	0.04	b.d.	b.d.	0.03	b.d.	0.04	0.08	b.d.	b.d.	b.d.	b.d.	0.09	b.d.	b.d.	
BaO	0.05	b.d.	0.07	0.05	b.d.	b.d.	b.d.	b.d.	b.d.	0.08	b.d.	0.26	b.d.	0.09	b.d.	b.d.	0.04	b.d.	
SrO	0.04	b.d.	0.25	0.11	0.14	0.09	b.d.	0.23	0.17	n.a.	n.a.	n.a.	n.a.	n.a.	n.a.	n.a.	n.a.	n.a.	
CaO	0.01	63.4	63.6	63.4	63.7	64.5	64.3	64.7	64.3	63.9	64.3	63.6	64.5	64.0	62.7	64.1	63.6	63.5	65.1
Na_2O	0.03	0.62	0.36	0.46	0.51	0.59	0.59	0.22	0.44	0.23	0.51	0.33	0.20	0.33	0.33	0.38	0.44	0.38	
K_2O	0.01	0.13	0.10	0.08	0.11	0.07	0.07	0.03	0.06	0.09	0.18	0.12	0.05	0.11	0.06	0.13	0.14	0.11	
P_2O_5	0.02	1.92	1.27	1.02	1.56	1.76	1.45	0.63	1.20	0.72	1.30	0.89	0.45	0.88	0.51	0.99	0.96	0.82	
SO_3	0.03	0.06	b.d.	b.d.	b.d.	0.04	0.05	0.14	0.10	b.d.	0.07	b.d.	b.d.	0.04	0.15	b.d.	b.d.	0.06	
Total	–	100.0	99.8	99.5	99.9	100.3	100.0	100.0	100.0	99.7	99.7	99.8	99.8	99.9	98.9	100.3	99.6	99.6	100.0
Cations calculated on the basis of 4 oxygens $M_2[TO_4]$, in apfu																			
Ca		1.94	1.96	1.95	1.96	1.97	1.98	1.99	1.98	1.97	1.98	1.95	1.98	1.97	1.94	1.95	1.96	1.95	2.00
Na		0.03	0.02	0.03	0.03	0.03	0.03	0.01	0.02	0.01	0.03	0.02	0.01	0.02	0.02	0.02	0.02	0.02	
K		0.00	0.00	0.00	0.00	0.00	0.00	0.00	0.00	0.00	0.01	0.00	0.00	0.00	0.00	0.00	0.00	0.00	
Mg+Fe+Sr+Ba		0.00	0.01	0.01	0.01	0.00	0.01	0.01	0.01	0.02	0.01	0.02	0.00	0.01	0.01	0.00	0.00	0.00	
Σ[M]		1.98	1.99	1.99	1.99	2.01	2.02	2.01	2.01	2.00	2.02	2.00	2.00	2.00	1.96	1.98	1.99	1.98	
Si		0.95	0.97	0.98	0.96	0.94	0.95	0.96	0.95	0.96	0.95	0.97	0.99	0.97	0.99	0.98	0.98	0.98	1.00
P		0.05	0.03	0.02	0.04	0.04	0.04	0.02	0.03	0.02	0.03	0.02	0.01	0.02	0.01	0.02	0.02	0.02	
Al+S+Ti+V		0.01	0.01	0.00	0.01	0.01	0.01	0.01	0.01	0.02	0.01	0.01	0.00	0.01	0.03	0.00	0.00	0.01	
Σ[T]		1.01	1.00	1.01	1.00	0.99	0.99	0.99	1.00	1.00	0.99	1.00	1.00	1.00	1.02	1.01	1.01	1.01	

Notes: b.d. = below detection; n.a. = not analyzed; n = number of analyses.

Table 6. Composition of ye'elimite (wt%)

Sample		YV-411				YV-412					YV-413			
	LLD				average n=3					average n=10				average n=6
SiO_2	0.03	0.91	0.76	0.88	0.85	1.80	0.48	0.42	0.54	0.81	0.70	0.73	0.77	0.73
TiO_2	0.02	b.d.	0.04	0.06	0.04	0.04	b.d.	b.d.	b.d.	b.d.	0.03	0.05	b.d.	0.03
Al_2O_3	0.02	45.6	46.9	46.9	46.5	46.2	47.6	48.0	47.8	47.4	47.9	47.3	46.0	47.1
Fe_2O_3-total	0.02	2.71	2.90	2.76	2.79	2.29	2.17	2.11	1.93	2.13	1.80	2.14	1.83	1.92
MgO	0.02	b.d.	b.d.	b.d.	b.d.	0.04	b.d.	b.d.	b.d.	b.d.	0.08	0.07	0.07	0.07
V_2O_5	0.03	b.d.	b.d.	b.d.	b.d.	b.d.	b.d.	b.d.	b.d.	b.d.	0.06	0.08	b.d.	0.05
BaO	0.05	0.94	0.66	0.71	0.77	0.13	0.07	0.13	0.18	0.13	0.26	0.26	0.34	0.29
SrO	0.04	0.20	0.47	0.29	0.32	0.37	0.32	0.30	0.46	0.36	b.d.	b.d.	b.d.	b.d.
CaO	0.01	35.2	35.5	35.6	35.5	36.9	36.0	36.0	36.3	36.3	35.5	36.0	35.5	35.7
Na_2O	0.03	0.23	0.15	0.19	0.19	0.17	0.12	0.11	0.16	0.14	0.05	0.07	0.15	0.09
K_2O	0.01	0.73	0.12	0.12	0.32	0.06	0.04	0.04	0.05	0.05	0.12	0.10	0.20	0.14
P_2O_5	0.02	0.20	0.30	0.23	0.24	0.09	0.03	0.06	0.08	0.06	0.26	0.23	0.18	0.22
SO_3	0.03	12.5	11.2	11.7	11.8	11.2	12.1	12.0	12.2	11.9	11.8	12.1	12.7	12.2
Total	–	99.2	99.0	99.4	99.3	99.3	98.9	99.2	99.7	99.3	98.6	99.1	97.7	98.5
Formula based on 16 oxygens $M_4[T_6O_{12}][XO_4]$, in apfu														
Ca		3.94	3.99	3.98	3.97	4.13	4.01	4.00	4.02	4.04	3.95	4.00	3.99	3.98
Ba		0.04	0.03	0.03	0.03	0.01	0.00	0.01	0.01	0.01	0.01	0.01	0.01	0.01
Sr		0.01	0.03	0.02	0.02	0.02	0.02	0.02	0.03	0.02	0.00	0.00	0.00	0.00
Na		0.05	0.03	0.04	0.04	0.03	0.02	0.02	0.03	0.03	0.01	0.01	0.03	0.02
K		0.10	0.02	0.02	0.04	0.01	0.01	0.00	0.01	0.01	0.02	0.01	0.03	0.02
Σ[M]		4.14	4.10	4.08	4.10	4.20	4.06	4.05	4.09	4.10	4.00	4.05	4.07	4.04
Al		5.62	5.80	5.76	5.73	5.68	5.84	5.87	5.83	5.80	5.87	5.78	5.69	5.78
Si		0.10	0.08	0.09	0.09	0.19	0.05	0.04	0.06	0.08	0.07	0.08	0.08	0.08
Fe^{3+}		0.21	0.23	0.22	0.22	0.18	0.17	0.16	0.15	0.17	0.14	0.17	0.14	0.15
V+Ti+Cr		0.00	0.00	0.00	0.00	0.00	0.00	0.00	0.00	0.00	0.02	0.01	0.01	0.01
Σ[T]		5.93	6.11	6.08	6.04	6.05	6.06	6.08	6.03	6.05	6.10	6.03	5.92	6.02
P		0.02	0.03	0.02	0.02	0.01	0.00	0.01	0.01	0.01	0.02	0.02	0.02	0.02
S		0.98	0.89	0.91	0.93	0.88	0.94	0.94	0.94	0.93	0.92	0.94	1.00	0.96
Σ[X]		1.00	0.91	0.93	0.95	0.89	0.95	0.94	0.95	0.93	0.94	0.96	1.02	0.98

Notes: b.d. = below detection; n.a. = not analyzed; n = number of analyses.

Table 7. Composition of fluorellestadite and fluorapatite (wt%)

Sample		YV-411				YV-412				YV-413				
Phase	LLD	Fluorapatite			average n=8	Fluorellestadite			average n=11	Fluorellestadite			Fluorapatite	
SiO_2	0.03	5.64	5.48	9.11	6.52	14.2	14.0	13.9	14.0	9.56	9.44	10.5	6.81	8.20
TiO_2	0.02	b.d.	b.d.	b.d.	b.d.	0.07	b.d.	0.07	0.06	0.05	0.06	0.05	0.06	0.03
Al_2O_3	0.02	0.05	b.d.	b.d.	b.d.	0.10	b.d.	b.d.	0.03	0.06	b.d.	0.11	b.d.	b.d.
FeO-total	0.02	0.07	0.10	0.33	0.13	0.10	0.07	0.07	0.10	0.16	0.18	0.16	0.04	0.11
MgO	0.02	b.d.	b.d.	b.d.	b.d.	b.d.	b.d.	b.d.	b.d.	0.06	b.d.	0.04	b.d.	0.06
V_2O_5	0.03	0.56	0.58	0.45	0.52	0.14	0.12	0.15	0.16	0.31	0.43	0.32	0.45	0.49
BaO	0.05	0.06	0.06	0.08	0.06	b.d.	b.d.	b.d.	b.d.	0.23	0.11	0.10	b.d.	0.15
SrO	0.04	0.17	0.24	0.24	0.24	0.19	0.26	0.34	0.26	n.a.	n.a.	n.a.	n.a.	n.a.
Cr_2O_3	0.02	n.a.	n.a.	n.a.	n.a.	n.a.	n.a.	n.a.	n.a.	0.02	0.19	0.20	0.19	0.10
CaO	0.01	56.0	56.2	56.0	56.2	56.7	56.5	56.5	56.5	55.3	55.0	55.7	55.6	55.0
Na_2O	0.03	b.d.	b.d.	b.d.	b.d.	0.07	0.06	0.07	0.06	0.06	0.09	0.04	0.07	0.04
K_2O	0.01	0.02	b.d.	b.d.	b.d.	0.02	b.d.	0.02	b.d.	b.d.	b.d.	0.03	0.03	0.03
P_2O_5	0.02	28.3	28.1	21.2	26.3	10.7	11.5	11.2	10.9	19.4	19.4	17.1	25.6	21.7
SO_3	0.03	8.20	7.82	11.5	9.01	16.5	16.4	16.6	16.3	12.2	11.9	13.17	8.38	11.0
F	0.06	2.72	2.68	2.88	2.82	2.85	2.52	2.77	2.83	3.15	3.45	3.11	2.90	3.06
Cl	0.01	n.a.	n.a.	n.a.	n.a.	n.a.	n.a.	n.a.	n.a.	0.03	b.d.	0.02	0.03	0.03
Total	–	101.8	101.3	101.8	101.8	101.6	101.4	101.7	101.2	100.6	100.3	100.7	100.2	100.0
$O=(F,Cl)_2$	–	1.14	1.13	1.21	1.19	1.20	1.06	1.17	1.19	1.33	1.46	1.32	1.23	1.30
Total	–	100.7	100.1	100.6	100.6	100.4	100.4	100.5	100.0	99.3	98.8	99.3	98.9	98.7
Cations calculated on the basis of 10 Ca atoms $M_{10}[ZO_4]_6X_2$, in apfu														
Ca		9.94	9.93	9.90	9.92	9.93	9.94	9.91	9.92	9.90	9.89	9.90	9.91	9.90
Sr		0.02	0.02	0.02	0.02	0.02	0.02	0.03	0.03	0.02	0.01	0.01	0.00	0.01
Fe		0.01	0.01	0.05	0.02	0.01	0.01	0.01	0.01	0.02	0.02	0.02	0.01	0.02
Mg		0.00	0.00	0.00	0.00	0.00	0.00	0.00	0.00	0.01	0.01	0.01	0.00	0.02
Na		0.00	0.00	0.00	0.00	0.02	0.02	0.02	0.02	0.00	0.00	0.01	0.01	0.01
Σ[M]		9.96	9.96	9.97	9.97	9.98	9.99	9.98	9.98	9.97	9.94	9.95	9.94	9.95
Si		0.93	0.90	1.50	1.07	2.32	2.29	2.28	2.29	1.60	1.58	1.74	1.13	1.38
P		3.96	3.91	2.96	3.66	1.47	1.60	1.55	1.51	2.75	2.75	2.40	3.59	3.08
S		1.02	0.97	1.42	1.11	2.02	2.02	2.04	2.00	1.53	1.50	1.64	1.05	1.39
Ti		0.00	0.00	0.00	0.00	0.01	0.00	0.01	0.01	0.01	0.01	0.01	0.01	0.00
Al		0.01	0.00	0.00	0.00	0.02	0.00	0.00	0.01	0.01	0.00	0.02	0.00	0.00
Cr		0.00	0.00	0.00	0.00	0.00	0.00	0.00	0.00	0.00	0.02	0.03	0.02	0.01
V		0.03	0.03	0.03	0.03	0.01	0.01	0.01	0.01	0.00	0.01	0.00	0.00	0.00
Σ[Z]		5.96	5.82	5.91	5.88	5.85	5.92	5.89	5.82	5.90	5.88	5.83	5.81	5.87
F		1.42	1.40	1.50	1.47	1.47	1.31	1.43	1.47	1.66	1.83	1.63	1.52	1.63
Cl		0.00	0.00	0.00	0.00	0.00	0.00	0.00	0.00	0.01	0.00	0.01	0.01	0.01
Σ[X]		1.42	1.40	1.50	1.47	1.47	1.31	1.43	1.47	1.67	1.83	1.64	1.53	1.63

Notes: n.a. = not analyzed; n = number of analyses.

Table 8. Composition of opaque minerals (wt%)

Sample		YV-411		YV-412	YV-413		
Mineral	LLD	1	2	3	4	5	6
SiO_2	0.01	n.a.	2.67	1.93	0.71	0.70	b.d.
TiO_2	0.01	0.33	17.9	2.99	2.12	16.1	0.40
Al_2O_3	0.02	16.4	4.7	9.09	10.3	5.22	19.3
Fe_2O_3-total	0.02	58.8	30.9	40.9	40.6	35.1	55.8
MnO	0.02	0.46	0.54	b.d.	b.d.	n.a.	n.a.
MgO	0.02	19.8	0.45	0.63	0.86	0.21	21.4
NiO	0.02	0.41	n.a.	n.a.	n.a.	n.a.	n.a.
ZnO	0.03	0.81	n.a.	n.a.	n.a.	n.a.	n.a.
Cr_2O_3	0.02	0.8	b.d.	0.66	0.19	0.06	1.63
CaO	0.01	1.23	42.8	42.8	44.6	42.2	0.45
Na_2O	0.03	0.09	n.a.	n.a.	0.07	0.16	0.07
K_2O	0.01	b.d.	n.a.	n.a.	0.04	0.04	b.d.
P_2O_5	0.02	b.d.	n.a.	n.a.	0.04	b.d.	0.03
Total	–	99.1	100.0	99.0	99.5	99.8	99.1

Notes: b.d. = below detection; n.a. = not analyzed; 1, 6 = Magnesioferrite, 2, 5 = Fe-analog of shulamitite, 3, 4 = Brownmillerite

Table 9. Comparison of typical compositions of calcium sulfoaluminate (CSA), belite-based calcium sulfoaluminate (BSA) cements and natural ye'elimite-larnite rocks (vol%)

Phase	CSA (Zhang et al. 1999)		CSA (Mehta 1978, 1980)	BSA (Gartner and Li 2006)		YL rocks
	Low ferrite percentages	High ferrite percentages	Ye'elimite-rich	Optimal composition	Composition range	Composition range
Ca_2SiO_4	15-30	15-35	45	45-65 α'-Ca_2SiO_4	40-70	35-50
Ye'elimite	55-75	35-55	20	20-30	15-35	15-20
Calcium alumoferrites	3-6	15-30	15	15-35	5-25	7-15
Anhydrite	–	–	20	–	–	–
Fluorapatite - Fluorellestadite	–	–	–	–	–	15-20
Other phases	–	–	–	0.1-10	0.1-10	2-10

Table 10. Thermal history reconstruction for ye'elimite-larnite rocks

Evidence from natural YL rocks	Interpretation after Campbell (1999) and references therein
Phase reactions during combustion metamorphism (melting or solid-state)	
• Dense structure of rocks; closed pore system; scanty ropes • Uniformly distributed main phases, including prismatic brownmillerites and Fe-analogs of shulamitite • Subhedral larnites and ye'elimites, rather uniform in size (10-30 µm) • No larnite (belite) clusters, dense or tightly packed with very little interstitial material • No small, satellite larnites (belites) formed by partial melting • No dendritic crystals of both larnite (belite) and Ca ferroaluminate • No typical eutectic intergrowths of ferrites and/or aluminates	• No evidence of melting • Solid state reactions • Densification below T_{melt} of the whole rock • No liquid at the time of larnite precipitation
• Predominant β - Ca_2SiO_4 polymorph • Homogeneous and rather coarse larnites, ye'elimites, fluorellestadites, and fluorapatites; no chemical zonality; uniformly distributed Fe, Al, Na, K, and P impurities • Prismatic ferrites • Rounded β - Ca_2SiO_4 grains • No larnite (belite) nests • Relatively coarse (up to 45 µm) larnites (belites) • No or few α´ - Ca_2SiO_4 grains	• Moderate to slow cooling rate within the range of extreme temperatures (1420 – 1300 °C) • Prolonged heating below liquid-formation temperature (about 1400 °C)
• Relatively low chemical impurities in β - Ca_2SiO_4 (2-3 wt% in total) unlike the primary α - Ca_2SiO_4 polymorph which can concentrate up to 7 wt% of impurities; no zoned crystals with coexisting different Ca_2SiO_4 polymorphs (α- or α´ - Ca_2SiO_4 in core and β - Ca_2SiO_4 in rim)	• Relatively low heating temperatures, fast quenching
Cooling rate	
• Preserved α´ - Ca_2SiO_4	• Quenching above 1280 °C
• Alite (hatrurite) decomposed into CaO and Ca_2SiO_4; corroded alites	• Tempering (quenching)
• No large ragged belites • No belite overgrowths • Clear belites (of roughly 20 µm), no exsolved dotlike inclusions • Rounded belites without lamelli	• Fast cooling • Rapidly cooled clinker
• Structureless belites	• Extremely rapid quenching as in lab
• Larnites (belites) with polysynthetic twins after (100) or (010)	• Normal cooling rate as in Portland cement clinker production (~ 20º /min at 1200 ºC)
• Colorless larnite (type II belite) with parallel striations; polysynthetic twins after (100) or (010)	• Primary Ca_2SiO_4 held at α´ - form; heating below 1420 °C; fast cooling
• Large isolated ferrite and aluminate prismatic crystals	• Moderate cooling rate • Reducing conditions of heating
Redox regime of heating and cooling	
• No K-bearing sulfates; potassium incorporated into ye'elimite • High percentage of perovskite ($CaTiO_3$) endmember in ferrites; relatively abundant Fe-analog of shulamitite • Large isolated ferrite and aluminate prismatic crystals • K and Fe sulfide, pyrrhotite and Cu and Cu-Ag selenides	• Heating under extreme reducing to reducing conditions
• Brown or grey color of densely burned clinker	• Heating under reducing conditions, cooling at ≥ 1250 °C under reducing conditions, further cooling in air
• No crustified structures	• Heating under dry conditions
Raw material (protolith): grain size and homogeneity	
• Small hatrurite (alite) (≤ 15 µm) crystals with inclusions	• Fast heating of very fine (≤ 50 µm) raw material at relatively low temperatures
• Randomly distributed belites; no nests • No belite clusters, dense or tightly packed with very little interstitial material	• No relatively coarse quartz and/or feldspar grains (≥ 44 µm); well mixed raw materials • High-quality uniform heating of clinker